Watanabe, W., Yoshida, H., Hirose, A., Akashi, T., Takeshita, T., Kuroki, N., Shibata, A., Hongo, S., Hashiguchi, S., Konno, K., Kurokawa, M., 2013. Perinatal exposure to insecticide methamidophos suppressed production of proinflammatory cytokines responding to virus infection in lung tissues in mice. Biomed. Res. Int., 151807.

Xu, J., Futakuchi, M., Iigo, M., Fukamachi, K., Alexander, D.B., Shimizu, H., Sakai, Y., Furukawa, F., Uchino, T., Tokunaga, H., Nishimura, T., Hirose, A., Kanno, J., Tsuda, H., 2010. Involvement of macrophage inflammatory protein 1 alpha (MIP1alpha) in promotion of rat lung and mammary carcinogenic activity of nanoscale titanium dioxide particles administered by intra-pulmonary spraying. Carcinogenesis 31, 927–935.

Zhang, H., Wang, C., Chen, B., Wang, X., 2012. Daunorubicin-TiO_2 nanocomposites as a smart pH-responsive drug delivery system. Int. J. Nanomed. 7, 235–242.

Journal of Crystal Growth 405 (2014) 68–72

Contents lists available at ScienceDirect

Journal of Crystal Growth

journal homepage: www.elsevier.com/locate/jcrysgro

Influence of the solution volume on the growth of C_{60} nanowhiskers

Kun'ichi Miyazawa *, Chika Hirata, Takatsugu Wakahara

Fullerene Engineering Group, Materials Processing Unit, National Institute for Materials Science (NIMS), 1-1 Namiki, Tsukuba 305-0044, Ibaraki, Japan

ARTICLE INFO

Article history:
Received 6 May 2014
Received in revised form
20 July 2014
Accepted 21 July 2014
Communicated by: K. Deppert
Available online 10 August 2014

Keywords:
A1. LLIP method
A1. Growth control
B1. C_{60} nanowhisker
B1. Fullerene nanowhisker

ABSTRACT

The lengths and diameters of C_{60} nanowhiskers (C_{60}NWs) grown in solutions were investigated relative to the inner diameter of the glass bottle and the solution volume while maintaining the volumetric ratio of C_{60}-saturated toluene and isopropyl alcohol at 1:1. The mean lengths and diameters of the C_{60}NWs increased, and the distribution of the lengths and diameters broadened when increasing the solution volume. The mean crystal nucleus size of the C_{60}NWs was determined by analyzing the size dependence of C_{60}NWs on the solution volume. The lengths and diameters of C_{60}NWs asymptotically approach their upper limits when increasing the solution volume.

1. Introduction

Fullerene nanowhiskers (FNWs) are thin, needle-like crystals composed of fullerene molecules, such as C_{60}, C_{70}, $C_{60}[C(COOC_2H_5)_2]$, $Sc_3N@C_{80}$, and others [1–4]. The needle-like fullerene crystals with diameters below 1000 nm are known as fullerene nanowhiskers [2,3]. One-dimensional fullerene crystals are promising materials for optical, electrical and electronic devices, including superconductors [5–9], and controlling their size is essential. For example, the electrical resistivity of these materials decreases rapidly when decreasing the diameter of the C_{60}NWs [10,11]. The photoluminescence peak for the C_{60} microtubes shifts toward lower wavenumbers when decreasing their diameters [12]. Controlling the size of C_{60}NWs is also important during their mechanical applications because their Young's modulus changes relative to the diameter and aspect ratio (length/diameter) of the C_{60}NWs [13–15]. The growth of C_{60}NWs is influenced by the temperature, light, ratio of the poor solvent versus the good solvent for C_{60}, and concentration of water [16–19,22]. In our previous paper, the diameter of the C_{60}NWs was a linear function of the area of the liquid–liquid interface when the total volume of solvent is constant, while the inner diameter of glass bottle changes [20].

However, the length of the C_{60}NWs must also be controlled before any practical application. In the present paper, we will demonstrate how the length and diameter of C_{60}NWs change depending on the bottle size and the solution volume. These analytical results will elucidate the synthesis of C_{60}NWs with size control.

2. Experimental

A C_{60}-saturated toluene solution was prepared by dissolving C_{60} powder (99.5% MTR Ltd.) in toluene (non-dehydrated, Wako Pure Chemical Industries, Ltd., Osaka, Japan); the undissolved C_{60} powder was removed via syringe filter with 450-nm pores (Puradisc TM, Whatman Inc., Clifton, USA).

The C_{60}NWs were synthesized through a modified LLIP method. Five different sizes of transparent glass bottles were used, as shown in Fig. 1. For the LLIP method, a C_{60}-saturated toluene solution was poured into a glass bottle and an equal amount of isopropyl alcohol (IPA) was layered onto the C_{60}-saturated toluene solution. The glass bottle was capped and manually mixed by shaking the bottle 30 times in order to obtain homogeneous precipitation of embryo C_{60} crystals [16]; afterwards, the bottles were stored in an incubator at 15 °C for 8 days to obtain well-grown C_{60}NWs, avoiding the destabilization of C_{60}NWs by the impurity water contained in the solvents [19]. The synthesis of C_{60}NWs was repeated three times for each size of glass bottle. Table 1 shows the amount of C_{60}-saturated toluene solution and IPA with the sizes of the glass bottles.

The lengths and diameters of the C_{60}NWs were measured via scanning electron microscopy (SEM) (FIB-SEM Hitachi NB5000). In the SEM observations, all the C_{60}NWs were collected from the above three glass bottles with the same size and put into a glass bottle containing IPA. After a gentle manual mixing for homogenization,

* Corresponding author. Tel.: +81 298604528; fax: +81 298604667.
E-mail address: miyazawa.kunichi@nims.go.jp (K. Miyazawa).

http://dx.doi.org/10.1016/j.jcrysgro.2014.07.036
0022-0248/

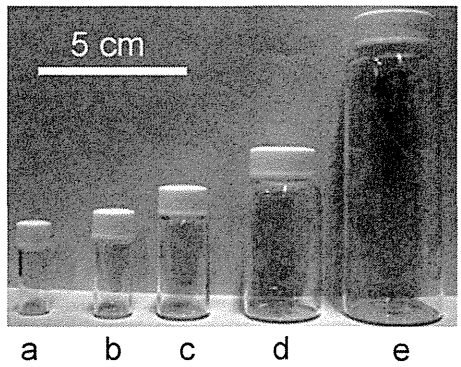

Fig. 1. Transparent glass bottles with inner diameters of (a) 10 mm, (b) 12.5 mm, (c) 18 mm, (d) 27 mm and (e) 36.5 mm, respectively.

Table 1
Inner diameters of the glass bottles, and the amounts of C_{60}-saturated toluene solution and IPA used during the synthesis of the C_{60}NWs.

Glass bottles (Fig. 1)	Inner diameter (mm)	C_{60}-saturated toluene solution (cm^3)	IPA (cm^3)	Solution volume (cm^3)
(a)	10.0	0.75	0.75	1.5
(b)	12.5	1.5	1.5	3.0
(c)	18.0	4.0	4.0	8.0
(d)	27.0	10.0	10.0	20.0
(e)	36.5	40.0	40.0	80.0

parts of the C_{60}NWs in the glass bottle were sampled onto a Si substrate for SEM observations. One hundred C_{60}NWs were visualized to measure their lengths and diameters using randomly selected SEM images.

3. Results and discussion

As shown in Fig. 2, short and straight C_{60}NWs with uniform diameters along their growth axes were successfully synthesized in each glass bottle. In the SEM images, finer C_{60}NWs are observed when the bottle size decreases. Figs. 3 and 4 show that the distributions of the length and diameter for the C_{60}NWs broaden when increasing the bottle size.

The mean lengths and diameters of the C_{60}NWs are plotted relative to the inner diameters of the bottles, as shown in Figs. 5 and 6. The mean length and diameter increase linearly when increasing the inner diameter of the glass bottle. The standard deviations for the length and inner diameter of C_{60}NWs increase, reflecting the broader distributions observed with the larger bottle sizes. Therefore, the uniformity of the C_{60}NWs depends on the size of the glass bottle and diverges when increasing the size of the glass bottle.

In addition, the length and diameter decrease when decreasing the bottle size. The *y*-intercepts are the smallest mean size of C_{60}NWs, which can be treated as the nucleus for crystal growth; these particles should have a mean length of 2.1 μm and a mean diameter of 305 nm. The C_{60} nuclei should have a mean aspect ratio of 6.9 (=2.1 μm/305 nm).

However, the aspect ratio for each C_{60}NW was calculated using the same data shown in Figs. 5 and 6. As shown in Fig. 7, the aspect ratio is observed to increase and broaden when increasing the inner diameter of the bottle. Fig. 8 shows the relationship between the mean aspect ratio and the inner diameter of the bottle. The smallest aspect ratio can be determined by using the *y*-intercept in Fig. 8; this value is 10.8. However, this value does not coincide with the value above (6.9). The large discrepancy between 10.8 and 6.9 in the aspect ratios indicates that the sizes of the C_{60}NW nuclei were estimated incorrectly, suggesting that the curve fittings were performed incorrectly. This result should have arisen from the fact that the above curve fittings were performed only for

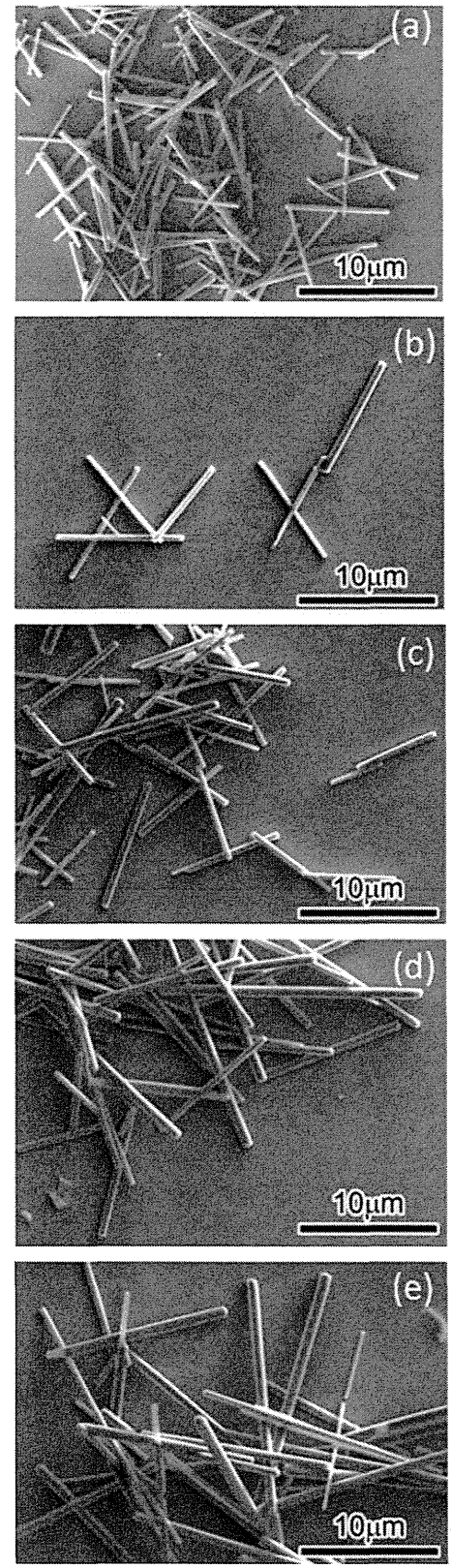

Fig. 2. SEM images of the C_{60}NWs synthesized using glass bottles with inner diameters of (a) 10 mm, (b) 12.5 mm, (c) 18 mm, (d) 27 mm and (e) 36.5 mm.

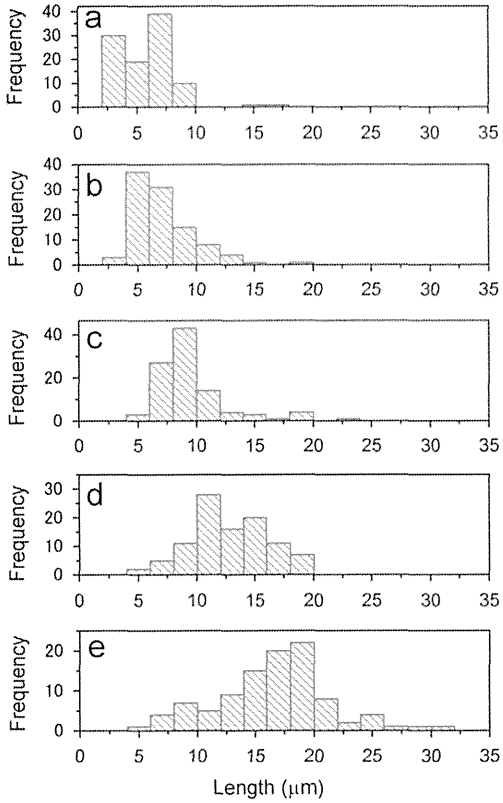

Fig. 3. Length distribution of the C_{60}NWs synthesized using glass bottles with inner diameters of (a) 10 mm, (b) 12.5 mm, (c) 18 mm, (d) 27 mm and (e) 36.5 mm, respectively.

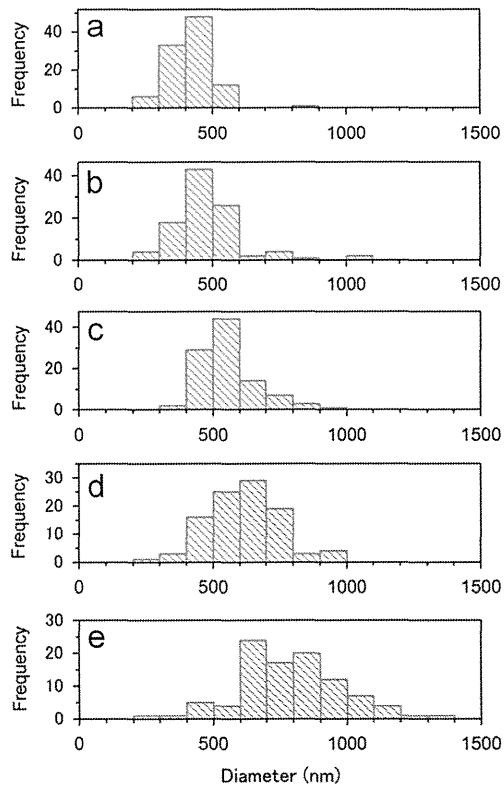

Fig. 4. Diameter distribution of the C_{60}NWs synthesized using glass bottles with inner diameters of (a) 10 mm, (b) 12.5 mm, (c) 18 mm, (d) 27 mm and (e) 36.5 mm, respectively.

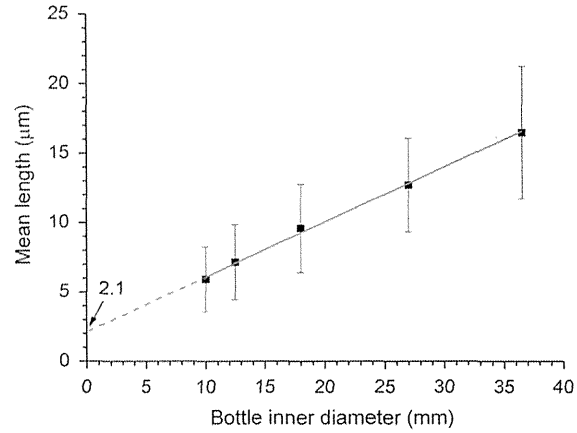

Fig. 5. Mean lengths of the C_{60}NWs (y) plotted relative to the inner diameter of the bottle (x). The fitted curve equation is $y=0.397x+2.1$.

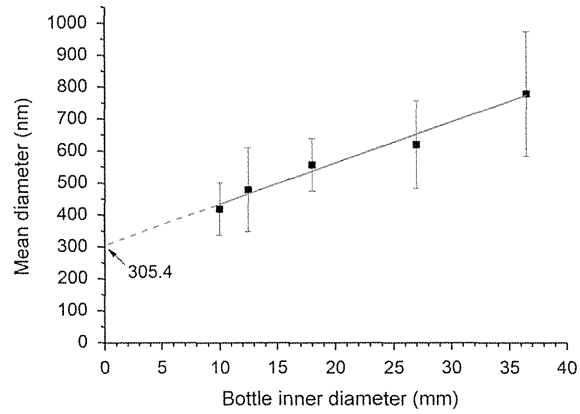

Fig. 6. Mean diameters of the C_{60}NWs (y) plotted relative to the inner diameter of the bottle (x). The fitted curve equation is $y=12.9x+305.4$.

the bottle's inner diameter and were not three-dimensionally performed. Therefore, analyses were also performed using the solution volumes, as shown in Figs. 9–11. The solution volume is defined as the arithmetic sum of the C_{60}-saturated toluene solution and IPA (Table 1).

The length, diameter and aspect ratio of the C_{60}NWs determined from the y-intercepts of Figs. 9–11 are 5.02 μm, 387 nm and 13.1, respectively. The aspect ratio is 5.02 μm/387 nm, producing an aspect ratio of 13.0. Because this value (13.0) is very close to 13.1, the size estimation using the solution volume must be correct. Therefore, the mean size of the C_{60}NW nuclei is estimated to be 5.02 μm long and 387 nm in diameter.

However, the fitted curves in Figs. 9 and 10 show that the mean length and diameter of C_{60}NWs approach the maximum values (16.6 μm and 784 nm, respectively). Therefore, the maximum mean size of the C_{60}NWs attained through the present synthetic method can be estimated from the data obtained after changing the solution volume.

Fig. 12 shows the relationship between the solution volume and the number of C_{60}NWs per unit volume (cm^3) (=number density) formed in the glass bottles. The number of C_{60}NWs in each glass bottle was calculated using the mean size of the C_{60}NWs in the glass bottle and the quantity of C_{60} powder dissolved in the glass bottle when using a saturated solution of C_{60} in toluene (2.58 mg cm^{-3} at 15 °C [21]). The number density of the C_{60}NWs in solution decreases linearly when increasing the solution volume in the double logarithmic plot. The highest number of nuclei per unit volume of solution may be estimated

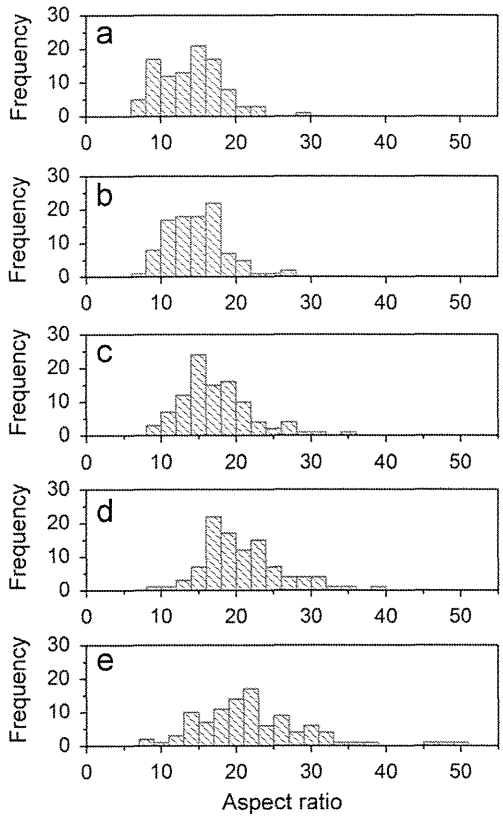

Fig. 7. Aspect ratio distributions of the C_{60}NWs for bottles with inner diameters of (a) 10 mm, (b) 12.5 mm, (c) 18 mm, (d) 27 mm and (e) 36.5 mm, respectively.

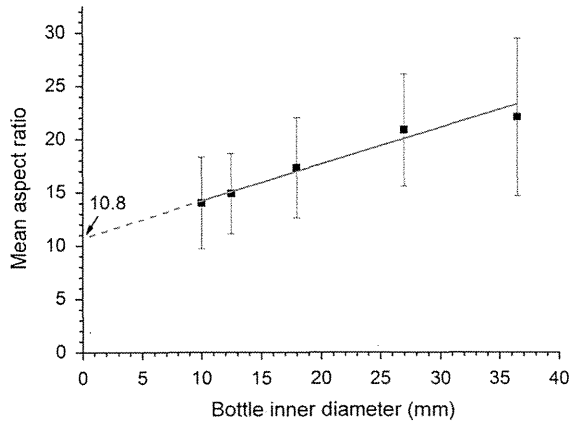

Fig. 8. Relationship between the mean aspect ratio of the C_{60}NWs (y) and the inner diameter of the glass bottles (x). The equation for the fitted curve is $y=0.343x+10.8$.

from the crystal nucleus size calculated for the C_{60}NWs (5.02 μm long and 387 nm in diameter); this value is 1.3×10^9 cm^{-3}. The fitted curve ($y=1.12496\times10^9/x^{0.5674}$) in Fig. 12 shows that the solution volume corresponding to the above number (1.3×10^9 cm^{-3}) is 0.77 cm^3. Therefore, the smallest C_{60}NWs can be obtained when the solution volume is below 0.77 cm^3 and when equal amounts of C_{60}-saturated toluene and IPA are used during the synthetic process.

However, the growth of C_{60}NWs changes depending not only on the solution volume but also on the combination of solvents used in the LLIP method. For example, tubular C_{60}NWs (C_{60} nanotubes) with lengths longer than several millimeters were synthesized, using a LLIP method combined with ultrasonication

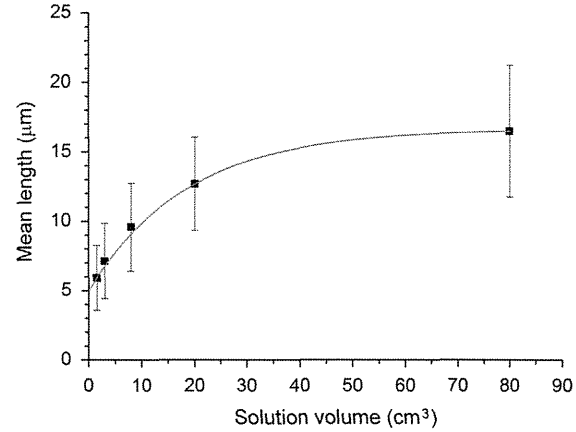

Fig. 9. Relationship between the solution volume (x) and the mean length of the C_{60}NWs (y). The equation for the fitted curve is $y=-11.6\exp(-x/18.7)+16.6$. The mean length asymptotically approaches 16.6 μm.

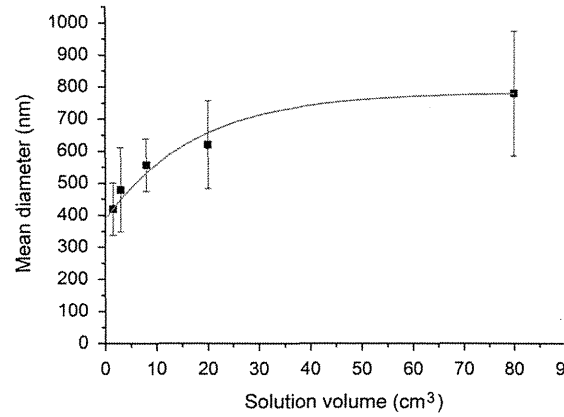

Fig. 10. Relationship between the solution volumes and the mean diameters of C_{60}NWs. The fitted curve equation is $y=-396.6\exp(-x/17.6)+783.7$. The mean diameter approaches 784 nm asymptotically.

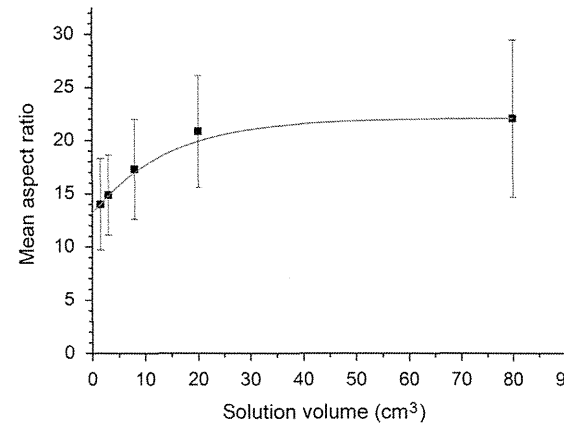

Fig. 11. Relationship between the solution volume (x) and the mean aspect ratio of the C_{60}NWs (y). The equation for the fitted curve is $y=-9\exp(-x/14.2)+22.1$. The mean aspect ratio approaches 22.1 asymptotically.

and manual mixing, where 1 mL of C_{60}-saturated pyridine solution and 9 mL of IPA were used [23]. In this case, although the solution volume was 10 cm^3, the length of C_{60}NWs far exceeds the size of the C_{60}NWs in the present experiment. Thus, in order to elucidate the growth mechanism of C_{60}NWs, how the combination of solvents influences the growth of C_{60}NWs is going to be investigated further.

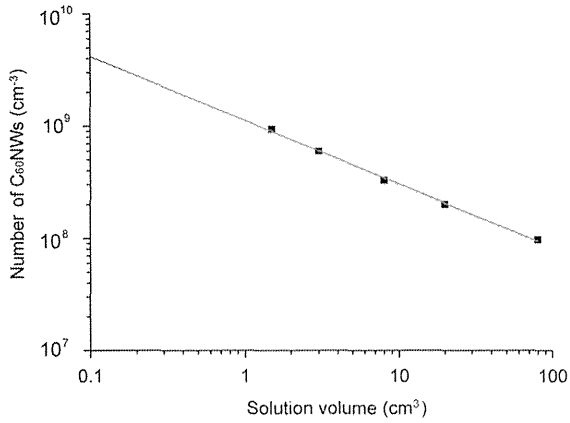

Fig. 12. Estimated number of C_{60}NWs per unit volume plotted versus the solution volume. The equation for the fitted curve is $y=1.12496\times10^{9}/x^{0.5674}$.

4. Conclusions

(1) The mean lengths and diameters of C_{60}NWs increase when increasing the bottle size. However, the size distribution of the C_{60}NWs broadens for the length and diameter when increasing the bottle size.
(2) The mean size of the C_{60}NW crystal nuclei can be determined from the *y*-intercepts for the mean diameters and lengths of the C_{60}NWs plotted versus the solution volume.
(3) The mean lengths, diameters and aspect ratios for the C_{60}NWs asymptotically approach their upper limits when increasing the solution volume.
(4) The number density of the C_{60}NWs in solution decreases when increasing the solution volume, revealing a linear relationship in their double logarithmic plot.
(5) The minimum size of the C_{60}NWs should be synthesized when the solution volume is below 0.77 cm^3.

Acknowledgments

Portions of this research were supported by the Health and Labor Sciences Research Grant (H24 - Chemistry - Shitei - 009) from the Ministry of Health, Labour and Welfare of Japan, and the JST Strategic Japanese-EU Cooperative Program "Study on managing the potential health and environmental risks of engineered nanomaterials".

References

[1] K. Miyazawa, Y. Kuwasaki, A. Obayashi, M. Kuwabara, J. Mater. Res. 17 (2002) 83.
[2] Fullerene Nanowhiskers, in: K. Miyazawa (Ed.), Pan Stanford Publishing Pte. Ltd., Singapore, 2011.
[3] K. Miyazawa, J. Nanosci. Nanotechnol. 9 (2009) 41.
[4] T. Wakahara, Y. Nemoto, M. Xu, K. Miyazawa, D. Fujita, Carbon 48 (2010) 3359.
[5] L.K. Shrestha, M. Sathish, J.P. Hill, K. Miyazawa, T. Tsuruoka, N.M. Sanchez-Ballester, I. Honma, Q. Ji, K. Ariga, J. Mater. Chem. C 1 (2013) 1174.
[6] L. Wei, J. Yao, H. Fu, ACS Nano 7 (2013) 7573.
[7] J Yang, H. Lim, H.C. Choi, H.S. Shin, Chem. Commun. 46 (2010) 2575.
[8] H. Takeya, K. Miyazawa, R. Kato, T. Wakahara, T. Ozaki, H. Okazaki, T. Yamaguchi, Y. Takano, Molecules 17 (2012) 4851.
[9] H. Takeya, R. Kato, T. Wakahara, K. Miyazawa, T. Yamaguchi, T. Ozaki, H. Okazaki, Y. Takano, Mater. Res. Bull. 48 (2013) 343.
[10] K. Miyazawa, Y. Kuwasaki, K. Hamamoto, S. Nagata, A. Obayashi, M. Kuwabara, Surf. Interface Anal. 35 (2003) 117.
[11] M.P. Larsson, J. Kjelstrup-Hansen, S. Lucyszyn, ECS Trans. 2 (2007) 27.
[12] S.I. Cha, K. Miyazawa, Y.K. Kim, D.Y. Lee, J.-D. Kim, J. Nanosci. Nanotechnol. 11 (2011) 3374.
[13] K. Asaka, R. Kato, K. Miyazawa, T. Kizuka, Appl. Phys. Lett. 89 (2006) 071912.
[14] K. Asaka, R. Kato, R. Yoshizaki, K. Miyazawa, T. Kizuka, Diam. Relat. Mater. 16 (2007) 1936.
[15] K. Saito, K. Miyazawa, T. Kizuka, Jpn. J. Appl. Phys. 48 (2009) 010217.
[16] K. Miyazawa, K. Hotta, J. Cryst. Growth 312 (2010) 2764.
[17] C.L. Ringor, K. Miyazawa, Diam. Relat. Mater. 17 (2008) 529.
[18] M. Tachibana, K. Kobayashi, T. Uchida, K. Kojima, M. Tanimura, K. Miyazawa, Chem. Phys. Lett. 374 (2003) 279.
[19] K. Miyazawa, K. Hotta, J. Nanopart. Res. 13 (2011) 5739.
[20] T. Wakahara, Y. Nemoto, M. Xu, K. Miyazawa, D. Fujita, Carbon 48 (2010) 3359.
[21] K.N. Semenov, N.A. Charykov, V.A. Keskinov, A.K. Piartman, A.A. Blokhin, A.A. Kopyrin, J. Chem. Eng. Data 55 (2010) 13.
[22] K. Hotta, K. Miyazawa, Nano 3 (2008) 355.
[23] K. Miyazawa, C. Ringor, Mater. Lett. 62 (2008) 410.

OPEN ACCESS
IOP Publishing | National Institute for Materials Science
Science and Technology of Advanced Materials
Sci. Technol. Adv. Mater. 16 (2015) 013502 (10pp)
doi:10.1088/1468-6996/16/1/013502

Review

Synthesis of fullerene nanowhiskers using the liquid–liquid interfacial precipitation method and their mechanical, electrical and superconducting properties

Kun'ichi Miyazawa

Fullerene Engineering Group, Materials Processing Unit, National Institute for Materials Science, Tsukuba, Ibaraki 305-0044, Japan

E-mail: miyazawa.kunichi@nims.go.jp

Received 27 November 2014, revised 14 January 2015
Accepted for publication 16 January 2015
Published 25 February 2015

Abstract

Fullerene nanowhiskers (FNWs) are thin crystalline fibers composed of fullerene molecules, including C_{60}, C_{70}, endohedral, or functionalized fullerenes. FNWs display *n*-type semiconducting behavior and are used in a diverse range of applications, including field-effect transistors, solar cells, chemical sensors, and photocatalysts. Alkali metal-doped C_{60} (fullerene) nanowhiskers (C_{60}NWs) exhibit superconducting behavior. Potassium-doped C_{60}NWs have realized the highest superconducting volume fraction of the alkali metal-doped C_{60} crystals and display a high critical current density (J_c) under a high magnetic field of 50 kOe. The growth control of FNWs is important for their success in practical applications. This paper reviews recent FNWs research focusing on their mechanical, electrical and superconducting properties and growth mechanisms in the liquid–liquid interfacial precipitation method.

Keywords: fullerene nanowhisker, fullerene nanotube, fullerene nanosheet, fullerene nanofiber, LLIP method, superconductor

1. Introduction

Fullerene molecules consist of closed cage-type structures that are composed of carbon atoms. The best-known fullerene is C_{60}, which was discovered by Kroto *et al* in 1985 [1]. The second well-known molecule is C_{70}, which was also identified in [1]. The C_{60} molecule is analogous to a soccer ball with 12 pentagons and 60 vertices where carbon atoms are located, and has 30 six-membered ring/six-membered ring joints with double bonds of carbon and 60 five-membered ring/six-membered ring joints with single bond of carbon.

Polymerization of C_{60} molecules can occur via [2+2] cycloaddition reactions, which form four-membered rings between adjacent C_{60} molecules. This cycloaddition mechanism involves a change of carbon hybridization from sp^2 to sp^3 [2].

Various properties of C_{60} have been studied by forming thin films on suitable substrates. Bulk samples can also be prepared by sintering at high temperatures. The [2+2] cycloaddition polymerization of C_{60} molecules is known to occur in the presence of ultraviolet or visible light illumination [3, 4], high-pressure sintering [5–8], and electron beam irradiation [9, 10]. The hardness of high-pressure sintered C_{60} reaches 200–300 GPa [11, 12].

However, fine needle-like crystals (whiskers) comprising C_{60}, 'C_{60} (fullerene) nanowhiskers (C_{60}NWs)', were found in

1468-6996/15/013502+10$33.00

a colloidal solution of lead zirconate titanate (PZT) with C_{60} added [13–15].

Fullerene nanofibers are linear and thin, with diameters less than 1000 nm [16, 17]. Fullerene nanosheets are thin two-dimensional substances. In this paper, we define fullerene nanosheets to be less than 1000 nm in thickness. Fullerene nanofibers and nanosheets can include a variety of fullerene molecules and their derivatives including C_{60}, C_{70}, $Sc_3N@C_{80}$ [18], $C_{60}[C(COOC_2H_5)_2]$ [19–21] and $(\eta^2\text{-}C_{60})Pt(PPh_3)_2$ [22].

The aspect ratio of fullerene nanofibers is defined to be greater than three [16]. Fullerene nanofibers are described as either non-tubular or tubular [23–27]. Non-tubular crystalline fullerene nanofibers are called fullerene nanowhiskers (FNWs). FNWs with both single-crystal and polycrystalline structures have been reported [53].

Fullerene nanofibers can incorporate either one or multiple types of fullerenes. This enables formation of both monocomponent and multicomponent structures. Examples of monocomponent structures include C_{60}NWs, C_{70} (fullerene) nanowhiskers (C_{70}NWs), C_{60} or C_{70} (fullerene) nanotubes (C_{60}NTs or C_{70}NTs), [23, 25, 28], and FNWs composed of $C_{60}[C(COOC_2H_5)_2]$ molecules ($C_{60}[C(COOC_2H_5)_2]$NWs). Examples of multicomponent fullerene nanofibers include two-component C_{60}–C_{70} NWs [29], two-component C_{60}–C_{70} NTs [23], two-component C_{60}–$C_{60}[C(COOC_2H_5)_2]$ NWs [19], and two-component C_{60}–$(\eta^2\text{-}C_{60})Pt(PPh_3)_2$ NWs [22]. Figure 1 shows the classification of fullerene nanofibers.

Fullerene nanofibers and nanosheets can be synthesized using the 'liquid–liquid interfacial precipitation (LLIP) method' [30], which has been widely applied [31–38]. In this review, we discuss the LLIP method to synthesize fullerene nanofibers and nanosheets and the applications in which these materials have been investigated.

The terminology 'FNW' represents all needle-like crystals comprising fullerene molecules with diameters less than 1000 nm. The words 'nanorod' and 'nanowire' are replaced with 'nanowhisker' to avoid confusion as was described in review paper [16].

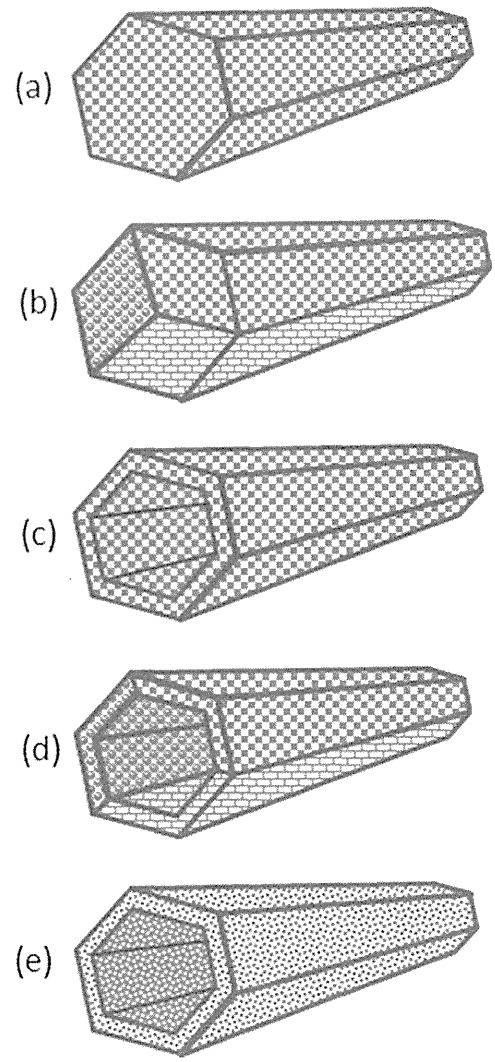

Figure 1. Classification of fullerene nanofibers. (a) single-crystal fullerene nanowhisker, (b) polycrystal fullerene nanowhisker, (c) single-crystal fullerene nanotube, (d) polycrystal fullerene nanotube, (e) amorphous fullerene nanotube.

2. Synthesis of FNWs

2.1. LLIP method

The LLIP method is commonly used to synthesize fullerene nanofibers and nanosheets [30]. This method relies on diffusion of a poor solvent of fullerenes such as isopropyl alcohol (IPA) into a fullerene-saturated toluene solution. An aliquot of a C_{60}-saturated toluene solution is added to a glass bottle. Following this, an appropriate amount of IPA is added gently to the solution to form a liquid–liquid interface [8]. The resulting mixture is kept at ambient temperatures, typically below 25 °C. During the slow mixing of toluene and IPA, the liquid–liquid interface becomes supersaturated in C_{60} and allows nucleation of C_{60}NWs to occur. This supersaturated state is maintained as IPA diffuses into toluene and assists in the growth of C_{60}NWs. This procedure is named 'static LLIP method' [30, 39]. The glass bottle is kept still in an incubator, where the C_{60}NWs self-assemble into a shape similar to a cotton ball. The LLIP method can also be used in combination with ultrasonic mixing, manual mixing, or injection [24, 39, 40]. Ultrasonication induces rapid mixing of good solvents and poor solvents, causing formation of fine fullerene nuclei that grow into fullerene nanofibers or nanosheets.

The static LLIP method can involve either layering a poor solvent onto a good solvent or vice versa, and can be combined with manual mixing, supersonic mixing, mixing by injection of liquid, or ultrasonic mixing of liquid droplets [41]. These methods are collectively named the 'dynamic LLIP method'.

Cha *et al* and Miyazawa *et al* reported the diaphragm LLIP method (DLLIP method), which involves injecting a poor solvent for fullerene into a fullerene solution through a porous membrane [40, 42, 43]. As an example, if IPA is slowly injected into a C_{60}-saturated toluene solution through

an anodic aluminum oxide membrane with nanosized pores, vertically grown microtubes of C_{60} are produced. All methods that mix two solvents to form fullerene nanofibers and nanosheets can be classified as LLIP processes.

Using the DLLIP method, the influence of alcohol chain length (methanol, ethanol, and IPA) on the length of C_{60} whiskers was investigated using toluene as a good solvent for C_{60}. Amer *et al* reported that the length of C_{60} whiskers decreased when the chain length of the alcohol (poor solvent) increased [44]. The temperatures at which the C_{60} whiskers were grown was not reported; however, the above result suggests that the chain length of the alcohol influences the desolvation energy of solvated C_{60} molecules that governs the rate-limiting process of surface reaction [45].

2.2. Growth mechanism of FNWs using the LLIP method

The Young modulus of C_{60}NWs has been examined using a transmission electron microscope equipped with an atomic force microscope [46]. The Young modulus of C_{60}NWs increases with decreasing diameter [46–49]. This phenomenon is thought to occur because C_{60}NWs have a core–shell structure with a porous interior region and a dense surface region [48, 50]. Kizuka *et al* found that C_{70}NWs containing solvent molecules had a higher density of lattice defects in their interior regions, which caused a reduction in the Young modulus [51]. Additionally, the Young modulus of C_{70}NTs was found to increase with decreasing diameter [25]. These studies conclude that by decreasing the diameter of fullerene nanofibers, crystallinity is increased, which in turn leads to an increase in the Young modulus.

In the LLIP process, FNWs grow from seed crystals [52–54]. The size of the initial C_{60}NW nuclei is influenced by the degree of supersaturation of C_{60} in solution, which is determined by the mixing ratio of both good and poor solvents [39]. C_{60}NTs grow in both directions along their growth axis from the seed crystals [53, 54]. However, the seed crystals should disappear by the core dissolution mechanism to form a through-hole structure [55].

The re-growth of C_{60}NTs was observed in ultrasonically pulverized C_{60}NTs [53]. The ultrasonically fractured C_{60}NTs have steep wall edges, on which C_{60} molecules accumulate and crystallize [53]. This preferential accumulation of C_{60} in areas with a small radius of curvature, such as the hexagonal vertices, is an important growth mechanism of fullerene nanotubes [53, 54].

The growth of C_{60}NWs is influenced by numerous factors, including time, temperature, light, solvent species, the ratio between good and poor solvents, and contained impurity water [39, 56–59]. The growth mechanism of C_{60}NWs in C_{60}-saturated toluene and IPA has been studied closely. The activation energy of growth (52.8 kJ mol^{-1}) was calculated by varying the temperature and measuring the length of C_{60}NWs. This value is approximately four times greater than the value obtained for the diffusion of C_{60} in a mixed solution of toluene and acetonitrile (13.1 kJ mol^{-1}, 4:1 v/v) [56, 60]. The high activation energy indicated that the growth of C_{60}NWs is rate limited by the desolvation process of C_{60} molecules bonded with solvent molecules on the crystal surface.

The dynamic LLIP process involves a fullerene solution being forcibly mixed with a poor solvent for fullerene. This process generates microscopic liquid–liquid interfaces between the fullerene solution and the poor solvent of fullerene, where supersaturated solutions lead to rapid nucleation of fine fullerene crystals. The formation of granular, linear, or sheet fullerene crystal morphologies depends on the growth kinetics, which may be governed by the degree of supersaturation, solvent species, and temperature.

Size control of fullerene nanofibers is critical for practical applications. Wakahara *et al* reported that the diameter of C_{60}NWs varied with the size of the glass bottles used in their synthesis. Linear relationships between the area of the liquid–liquid interface and the diameter of C_{60}NWs were observed when the total volume of solution was fixed [61]. Changes in the lengths and diameters of C_{60}NWs upon varying the solution volume have been examined [62]. These C_{60}NWs were prepared by dynamic LLIP in a C_{60}-saturated toluene and IPA system. After the initial formation of a liquid–liquid interface by layering an equal amount of IPA on a C_{60}-saturated toluene solution, the solution was manually mixed by shaking 30 times. The relationships between solution volume and mean length, diameter and aspect ratio are shown in figures 2(a)–(c) [62]. The aspect ratio, as derived from the *y*-intercepts of figures 2(a) and (b) (5.02 μm/387 nm) yielded a value of 13.0, almost identical to the value derived from the *y*-intercept of figure 2(c) (13.1). Hence, it is reasonable to consider the size of C_{60}NW nuclei can be estimated using the relationships shown in figures 2(a)–(c).

The relationship between the solution volume and number of C_{60}NWs per unit volume is shown in figure 2(d). The number density, as calculated from the nominal content of C_{60} and the mean size of C_{60}NWs in solution [62], increased as the solution volume decreased. This implies that the volume fraction of liquid–liquid interfaces increases when the solution volume is decreased. A power law relationship ($y = 1.12 \times 10^9 x^{-0.567}$) was fitted to the data with an approximate index of −0.5, showing that the number density of C_{60}NW nuclei in solution is inversely proportional to the square root of the solution volume.

A model describing the changes in the liquid–liquid interface upon manual mixing is shown in figure 3. The initial layered interface (figure 3(a)) is assumed to form a sinusoidally modulated interface (figure 3(b)) upon the manual mixing. The amplitude of this interface increases along the height of the glass bottle, a section of this wavefront is highlighted by the blue rectangle (figure 3(c)). This highlighted section is modeled by a cylinder with height h, radius r, basal area S, and volume V (figure 4(a)). The front of the liquid–liquid interface travels vertically with a velocity v.

The following equations hold.

$$V = Sh, \tag{1}$$

$$h = pr, \text{ where } p \text{ is a constant,} \tag{2}$$

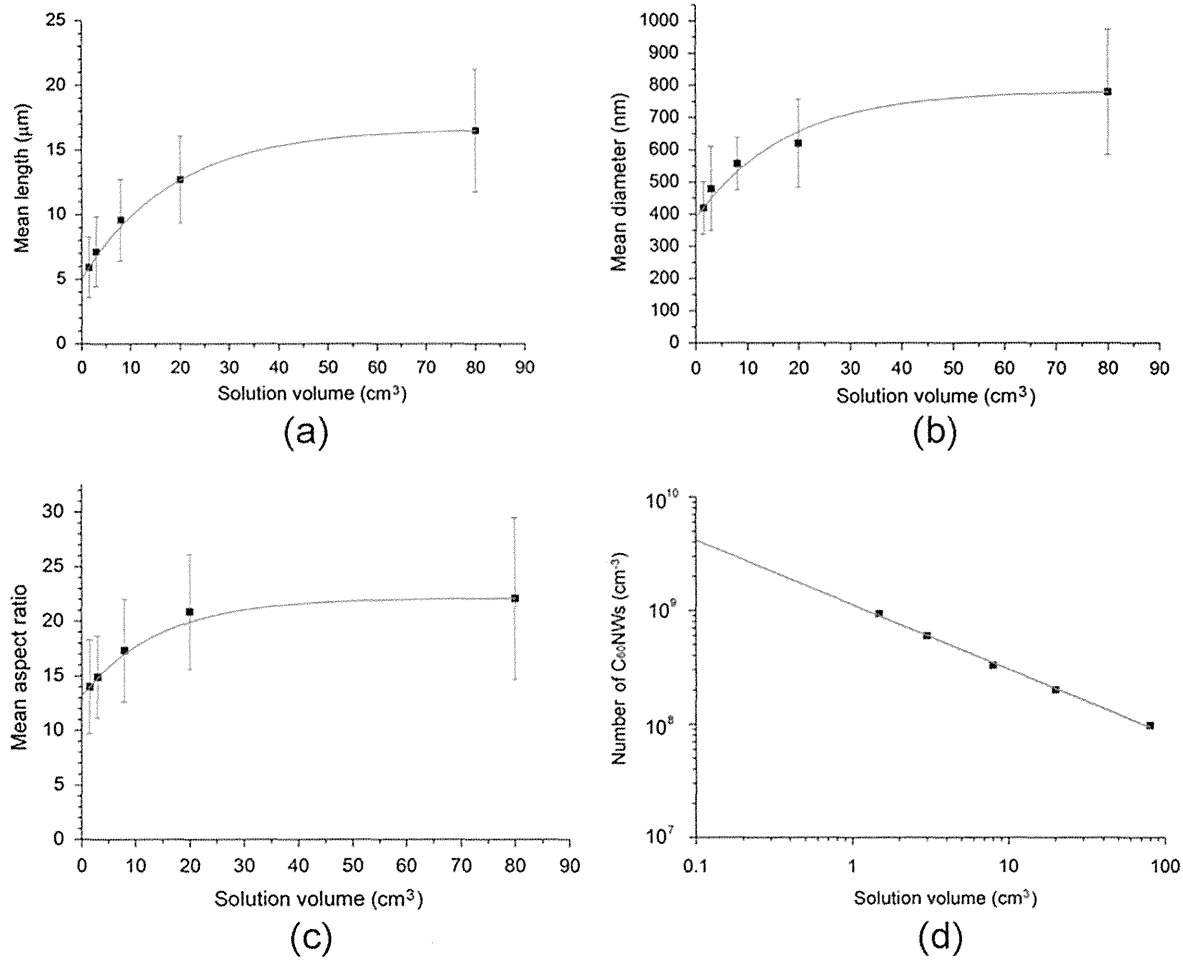

Figure 2. (a) Relationship between solution volume and mean length of C_{60}NWs. The equation fitted to the data is $y=-11.6\exp(-x/18.7)+16.6$. (b) Relationship between solution volume and mean diameter of C_{60}NWs. The equation fitted to the data is $y=-396.6\exp(-x/17.6)+783.7$. (c) Relationship between solution volume and the mean aspect ratio of C_{60}NWs. The equation fitted to the data is $y=-9\exp(-x/14.2)+22.1$. (d) Estimated number of C_{60}NWs per unit volume plotted versus the solution volume. The equation fitted to the data is $y=-1.12496\times10^{9}\,x^{-0.5674}$. Reprinted from [62], copyright 2014, with permission from Elsevier.

$$V = qS^{3/2}, \text{ where } q = p/\pi^{1/2}. \tag{3}$$

The front of liquid–liquid interface is assumed to move along the height h with a time t.

$$t = h/v. \tag{4}$$

As the liquid–liquid interface front moves, interdiffusion between C_{60}-satulated toluene solution and IPA occurs (figure 4(b)). If the values of both t and Δr are assumed to be small, the area of the interdiffusion zone (ΔS) is approximated as follows:

$$\Delta S = 2\pi r \Delta r. \tag{5}$$

The volume of interdiffusion ΔV is:

$$\Delta V = h\Delta S. \tag{6}$$

If Δr is assumed to be proportional to $(Dt)^{1/2}$ with a coefficient of interdiffusion D [63], it is calculated as in equation (7) with a constant a,

$$\Delta r = at^{1/2}. \tag{7}$$

Hence, combining (4), (5), and (7),

$$\Delta S = bh^{1/2}, \text{ where } b = 2\pi ra(1/v)^{1/2}. \tag{9}$$

If N is defined as the number of C_{60}NW nuclei per unit volume in the zone of interdiffusion, the mean number of C_{60}NW nuclei contained in a unit volume of a cylinder (ρ) can be calculated by combining equations (1), (3), (6), and (9):

$$\rho = (Nbq)V^{-1/2}. \tag{12}$$

This model suggests that the mean number density of C_{60}NW nuclei is inversely proportional to the square root of the solution volume, which was indeed confirmed experimentally (figure 2(d)).

3. Electrical and superconducting properties of C_{60}NWs

C_{60}NWs display n-type semiconducting behavior and are used in a diverse range of applications, including field effect

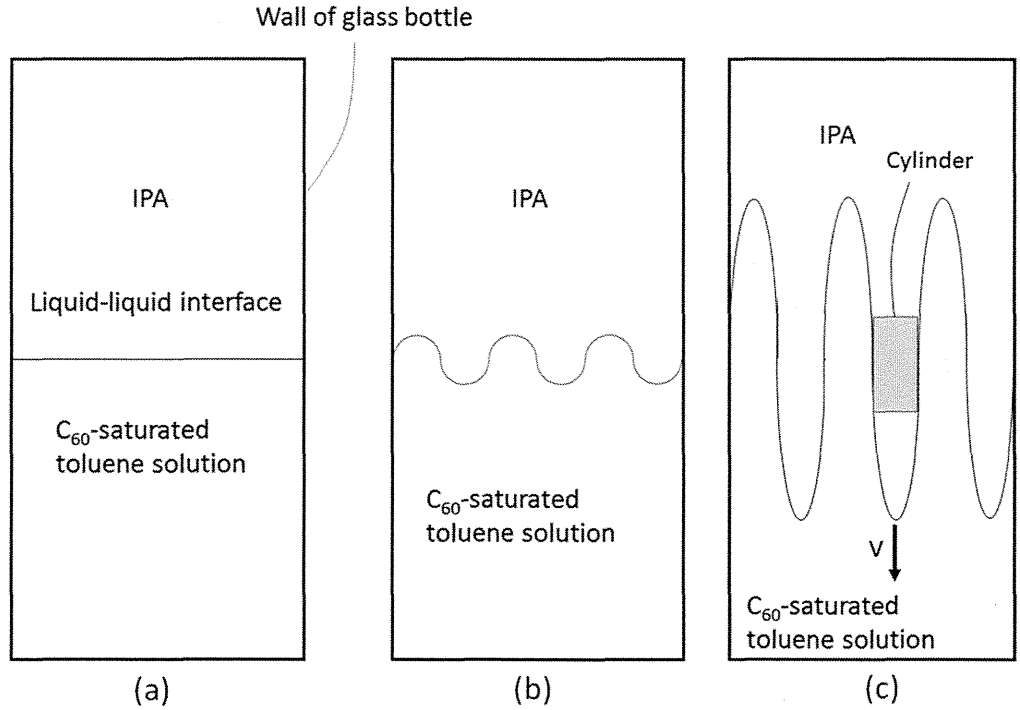

Figure 3. Model showing the liquid–liquid interface (a) changing with manual mixing (b). The interface front between the C_{60}-saturated toluene solution and IPA is assumed to move with a velocity v along the vertical direction of the glass bottle (c).

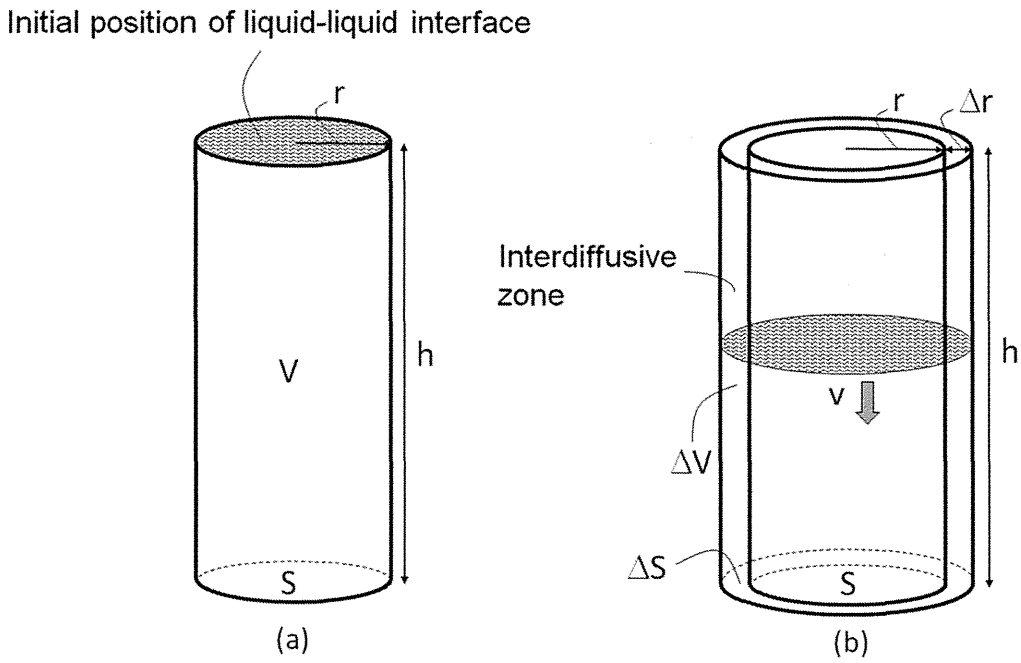

Figure 4. Cylindrical model used to calculate the number density N of C_{60}NW nuclei for the region of the liquid–liquid interface shown in figure 3(c).

transistors (FETs) [64], solar cells [65, 66], photocatalysts [67], chemical sensors [27], and photosensors [68]. However, Wakahara *et al* recently synthesized ambipolar FETs with C_{60}/cobalt–porphyrin hybrid nanosheets using a LLIP method [92].

The carrier mobility of C_{60}NWs in a FET was determined to be 2×10^{-2} cm^2 V^{-1} s^{-1} under vacuum [64]. However, the as-synthesized solution-grown C_{60} needle-like crystals exhibited a very high mobility up to 11 cm^2 V^{-1} s^{-1} [69]. As the measured carrier mobility of C_{60}NWs, or needle-like crystals of C_{60}, depends largely on the measurement conditions (solvent impurities, oxygen impurity, crystal structure, and lattice defects), electrical properties of the materials were investigated under controlled conditions. Only C_{60}NWs with clearly defined chemical and structural properties were used.

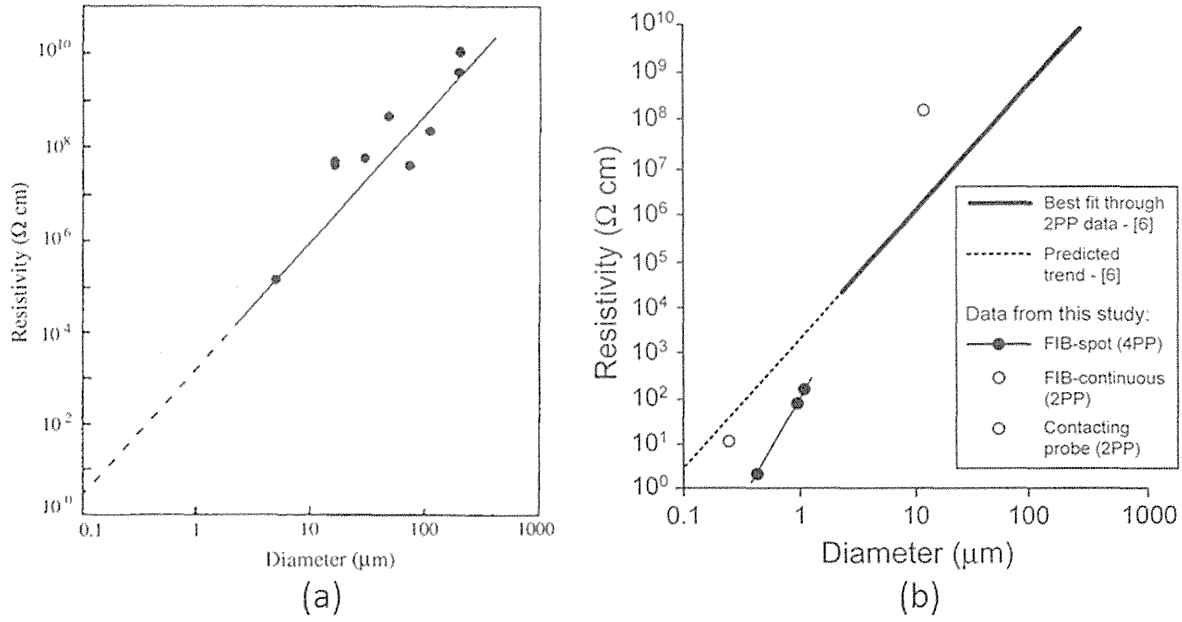

Figure 5. Electrical resistivity of C_{60} whiskers measured as a function of diameter. The resistivity measurement was performed by the two-point probe method (2PP) in (a) and by the four-point probe method (4PP) in (b). [6] in the inset of (b) is identical with [70]. FIB stands for focused ion beam. Part (a) reprinted with permission from [70], copyright © 2003 John Wiley & Sons, Ltd. Part (b) reproduced by permission of ECS—The Electrochemical Society from [71]

The electrical resistivity of C_{60} whiskers with diameters greater than 1 μm (~10–a few hundred micrometers) was measured using a two-terminal method at ambient temperature [70]. The electrical resistivity of the C_{60} whiskers decreased dramatically with decreasing diameter (figure 5(a)). The resistivity of C_{60}NWs is expected to be several Ohm centimeters (Ω cm), based on extrapolation of the curve-fitted data. Subsequently, Larsson *et al* measured the electrical resistivity using a four-point probe method [71]. Figure 5(b) summarizes their results including figure 5(a) [70]. The four-point probe method also showed a decrease in resistivity of C_{60} whiskers with decreasing diameter (FIB-spot (4PP)), figure 5(b)). A C_{60}NW with a diameter of 650 nm showed a low resistivity of 3 Ω cm [71]. The decrease in resistivity with decreasing diameter suggested that C_{60}NWs with smaller diameters and shorter C_{60} intermolecular distances are more crystalline and thus have a greater overlap of π electrons [70]. Recently, this fact was further confirmed by Barzegar *et al* using thinner C_{60}NWs [93]. It was shown that the electrical mobility of as-grown C_{60}NWs with diameters less than 300 nm increases with decreasing the diameter of C_{60}NWs [64, 93–95].

If the line measured using the four-point probe method is extrapolated to a diameter of 100 nm in figure 5(b), the resistivity will decrease to the order of 10^{-3} Ω cm. This result suggests that C_{60}NWs may exhibit metallic conductivity when their diameters are sufficiently small. Xu *et al* showed that C_{60}NWs are conductive only if the surface is not covered by oxygen [72].

To determine the electrical properties of a semiconductor, it is necessary to measure the temperature dependence of electrical conductivity. Ji *et al* performed these measurements using C_{60}NWs with either a face-centered cubic (fcc) or a hexagonal closed packed (hcp) structure [73]. The fcc C_{60}NW displayed higher electrical conductivity than did the hcp C_{60}NW. This result confirms that the crystal structure influences the electrical properties of C_{60}NWs. However, the effect of solvent molecules contained in the hcp C_{60}NW is still under some debate. If C_{60} molecules adopt a closely packed structure, a greater overlap between π electrons would lead to higher electrical conductivity in these C_{60}NWs [70, 73].

Carbon superconductors have been investigated for many years. The superconductivity of graphite (C_8) specimens doped with alkali metals, including K (superconducting transition temperature (T_c) < 0.55 K [74], 0.128–0.198 K [75]), Cs (T_c = 0.020–0.135 K [74]), and Rb (T_c = 0.023–0.151 K [74]) has been reported. Graphite superconductors such as C_6Ca (T_c = 11.5 K) and C_6Yb (T_c = 6.5 K) were also synthesized [76]. C_{60}NWs can be transformed into glassy carbon nanofibers by heat treatment [77–79]. When heated to 3000 °C, C_{60}NWs transform into carbon nanofibers with up to 17 graphene layers [77]. The number of stacked graphene layers increases with increasing temperature between 2000 and 3000 °C [77]. Those C_{60}NWs heated at high temperatures with developed graphitic ribbons are promising materials that may exhibit superconductivity if doped with alkali metals and alkaline-earth metals. In addition, the high-temperature-treated C_{60}NWs become electron emission tips showing striped patterns that reflect the atomic structure of the crumpled graphitic layers [78, 79]. However, since long amorphous carbon nanofibers prepared by high-

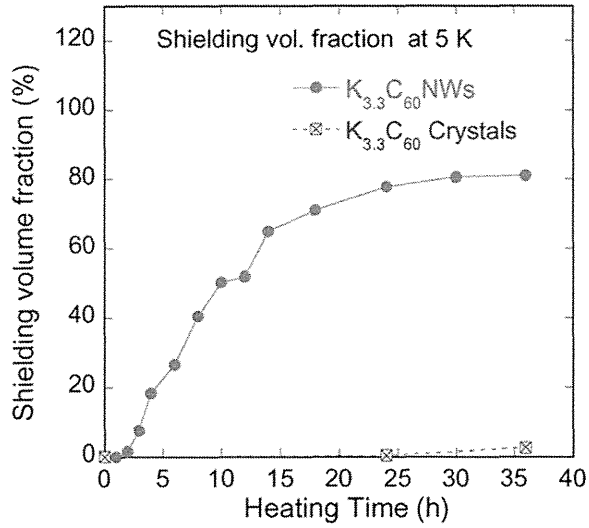

Figure 6. Shielding volume fractions in K-doped C_{60}NWs and K-doped C_{60} crystal powder (reprinted from [87]).

temperature heat treatment of C_{60}NWs showed cytotoxicity like long multiwall carbon nanotubes [96], special care will be necessary in the practical uses of the glassy carbon nanofibers.

In 2004, boron-doped diamond was observed to exhibit superconductivity ($T_c \approx 4$ K) [80]. Takano *et al* found that the T_c of a boron-doped diamond film was 7.4 K [81].

Hebard *et al* discovered that C_{60} doped with potassium (K) exhibited superconductivity [82]. A superconducting transition temperature (T_c) of 18 K was observed for both K-doped C_{60} films and bulk samples. Tanigaki *et al* reported the highest T_c value of 33 K in $Cs_2Rb_1C_{60}$ powder [83].

Of the three known phases of K-doped C_{60} (fcc (K_3C_{60}), body-centered tetragonal (bct) (K_4C_{60}), and body-centered cubic (bcc) (K_6C_{60})), only the fcc phase exhibits superconductivity [84]. Although C_{60}NWs that are grown in solution display a solvated hexagonal structure, they transform into an fcc structure upon drying and removal of the internal solvent molecules [85]. Hence, these fcc C_{60}NWs should be superconducting if doped with alkali metals [15]. C_{60} nanotubes were doped with Li, Na, and K, and the crystal structures were examined using Raman spectroscopy [86]. Superconductive C_{60}NWs were also successfully fabricated by doping with K [87, 88]. Although the T_c value (17 K) of the K-doped C_{60}NWs with a nominal composition of $K_{3.3}C_{60}$ was lower than the reported value of 18 K [82], the superconducting, shielding volume fraction was as high as 80%, and the critical current density J_c was more than 3×10^5 A cm^{-2} under 50 kOe [87, 88], although the doping was performed at 200 °C for 24 h. The shielding volume fraction of the K-doped C_{60} crystal powder was less than 1% when doped using the same process (figure 6). The high shielding volume fraction in the K-doped C_{60}NWs may allow for light, flexible, and recyclable superconducting carbon cables. Initially, the superconducting shielding volume fraction of K-doped C_{60} crystals was at most 35%, even after prolonged heat treatment (20 days) at temperatures up to 250 °C [89].

Efforts to increase the T_c value of alkali-doped C_{60}NWs are continuing. Values up to 26 K have been achieved by doping with Rb [90]. The volume fraction of Rb-doped C_{60}NWs was approximately five times greater than that of Rb-doped C_{60} powder. As Rb is an abundant alkali metal like the other common metals such as copper, lead, or zinc [91], lightweight Rb-doped C_{60}NWs are expected to find use in a variety of superconducting applications, including motor cars, cables for power delivery, and wind generators.

4. Summary

A variety of fullerene nanofibers and nanosheets have been synthesized using LLIP methods. These materials have found use in a wide range of applications, including solar cells, chemical sensors, photo sensors, photocatalysts, and ambipolar field-effect transistors. The synthesis of C_{60}NWs using a dynamic LLIP method with a C_{60}-saturated toluene solution and IPA suggests that nucleation is governed by the volume of the liquid–liquid interface produced by interdiffusion between the two solvents.

Alkali-metal-doped C_{60}NWs are the first carbon fibers to display superconductivity while being lightweight and flexible. K- or Rb-doped C_{60}NWs are promising superconductors with T_c values that are higher than those of any other practically used metal superconductors. Additionally, they are composed of non-toxic, abundant, and recyclable elements. Fullerene nanomaterials show great promise for a variety of applications in electrical and optical fields.

Acknowledgments

This research was supported by the Health and Labour Sciences Research Grants (H24-Chemistry-Shitei-009) from the Ministry of Health, Labour and Welfare of Japan, the JST Strategic Japanese-EU Cooperative Program 'Study on managing the potential health and environmental risks of engineered nanomaterials', the Center of Materials Research for Low Carbon Emission of the National Institute for Materials Science, and the Japan Society for the Promotion of Science KAKENHI Grant No. 26600007.

References

[1] Kroto H W, Heath J R, O'Brien S C, Curl R F and Smalley R E 1985 C_{60}: buckminsterfullerene *Nature* **318** 162–3
[2] Okada S, Saito S and Oshiyama A 1999 New metallic crystalline carbon: three dimensionally polymerized C_{60} fullerite *Phys. Rev. Lett.* **83** 1986
[3] Rao A M *et al* 1993 Photoinduced polymerization of solid C_{60} film *Science* **259** 955–7
[4] Kato R and Miyazawa K 2012 Raman laser polymerization of C_{60} nanowhiskers *J. Nanotechnol.* **2012** 101243

[5] Iwasa Y *et al* 1994 New phases of C_{60} synthesized at high pressure *Science* **264** 1570

[6] Miyazawa K, Satsuki H, Kuwabara M and Akaishi M 2001 Microstructural analysis of high-pressure compressed C_{60} *J. Mater. Res.* **16** 1960–6

[7] Minato J, Miyazawa K, Suga T, Kanda H, Akaishi M, Yamaura K, Muromachi E and Kakisawa H 2005 Characterization of high-pressure sintered C_{60} nanowhiskers and C_{60} powder *J. Mater. Res.* **20** 742–6

[8] Miyazawa K, Akaishi M, Kuwasaki Y and Suga T 2003 Characterizing high-pressure compressed C_{60} whiskers and C_{60} powder *J. Mater. Res.* **18** 166–72

[9] Nakaya M, Nakayama T and Aono M 2004 Fabrication and electron-beam-induced polymerization of C_{60} nanoribbon *Thin Solid Films* **464–5** 327–30

[10] Miyazawa K, Minato J, Fujino M and Suga T 2006 Structural investigation of heat-treated fullerene nanotubes and nanowhiskers *Diam. Relat. Mater.* **15** 1143–6

[11] Popov M, Mordkovich V, Perfilov S, Kirichenko A, Kulnitskiy B, Perezhogin I and Blank V 2014 Synthesis of ultrahard fullerite with a catalytic 3D polymerization reaction of C_{60} *Carbon* **76** 250–6

[12] Blank V, Popov M, Pivovarov G, Lvova N, Gogolinsky K and Reshetov V 1998 Ultrahard and superhard phases of fullerite C_{60}: comparison with diamond on hardness and wear *Diam. Relat. Mater.* **7** 427–31

[13] Miyazawa K, Obayashi A and Kuwabara M 2001 C_{60} nanowhiskers in a mixture of lead zirconate titanate sol–C_{60} toluene solution *J. Am. Ceram. Soc.* **84** 3037–9

[14] Rauwerdink K, Liu J, Kintigh J and Miller G P 2007 Thermal, sonochemical, and mechanical behaviors of single crystal [60] fullerene nanotubes *Microsc. Res. Tech.* **70** 513–21

[15] Miyazawa K and Kuwabara M 2005 Fine carbon wires and methods for producing the same *US Patent* 6890505B2

[16] Miyazawa K 2009 Synthesis and properties of fullerene nanowhiskers and fullerene nanotubes *J. Nanosci. Nanotechnol.* **9** 41–50

[17] Miyazawa K (ed) 2011 *Fullerene Nanowhiskers* (Singapore: Pan Stanford Publishing Pte. Ltd)

[18] Wakahara T, Nemoto Y, Xu M, Miyazawa K and Fujita D 2010 Preparation of endohedral metallofullerene nanowhiskers and nanosheets *Carbon* **48** 3359–63

[19] Miyazawa K, Minato J, Mashino T, Nakamura S, Fujino M and Suga T 2006 Structural characterization of room-temperature synthesized fullerene nanowhiskers *Nukleonika* **51** (Suppl. 1) S41–8

[20] Miyazawa K, Mashino T and Suga T 2004 Liquid phase synthesis of the nanowhiskers of fullerene derivatives *Trans. Mater. Res. Soc. Japan* **29** 537–40

[21] Miyazawa K, Mashino T and Suga T 2003 Structural characterization of the $C_{60}[C(COOC_2H_5)_2]$ whiskers prepared by the liquid–liquid interfacial precipitation method *J. Mater. Res.* **18** 2730–5

[22] Miyazawa K and Suga T 2004 Transmission electron microscopy investigation of fullerene nanowhiskers and needle-like precipitates formed by using C_{60} and $(\eta^2\text{-}C_{60})Pt(PPh_3)_2$ *J. Mater. Res.* **19** 2410–4

[23] Miyazawa K, Minato J, Yoshii T, Fujino M and Suga T 2005 Structural characterization of the fullerene nanotubes prepared by the liquid–liquid interfacial precipitation method *J. Mater. Res.* **20** 688–95

[24] Miyazawa K and Ringor C 2008 Platinum chloride deposition into C_{60} nanotubes *Mater. Lett.* **62** 410–3

[25] Kizuka T, Miyazawa K and Tokumine T 2012 Young's modulus of single-crystal fullerene C_{70} nanotubes *J. Nanotechnol.* **2012** 969357

[26] Liu H *et al* 2002 Imaging as-grown [60] fullerene nanotubes by template technique *J. Am. Chem. Soc.* **124** 13370–1

[27] Zhang X, Qu Y, Piao G, Zhao J and Jiao K 2010 Reduced working electrode based on fullerene C_{60} nanotubes@DNA: characterization and application *Mater. Sci. Eng.* B **175** 159–63

[28] Kizuka T, Miyazawa K and Tokumine T 2012 Synthesis of oriented bundle fibers of fullerene C_{70} crystal nanotubes *J. Nanosci. Nanotechnol.* **12** 2825–8

[29] Miyazawa K, Fujino M, Minato J, Yoshii T, Kizuka T and Suga T 2004 Structure and properties of fullerene nanowhiskers prepared by the liquid–liquid interfacial precipitation method *Proc. SPIE* **5648** 224

[30] Miyazawa K, Kuwasaki Y, Obayashi A and Kuwabara M 2002 C_{60} nanowhiskers formed by the liquid–liquid interfacial precipitation method *J. Mater. Res.* **17** 83–8

[31] Osonoe K, Kano R, Miyazawa K and Tachibana M 2014 Synthesis of C_{70} two-dimensional nanosheets by liquid–liquid interfacial precipitation method *J. Cryst. Growth* **401** 458- 461

[32] Wakahara T, Sathish M, Miyazawa K, Hu C, Tateyama Y, Nemoto Y, Sasaki T and Ito O 2009 Preparation and optical properties of fullerene/ferrocene hybrid hexagonal nanosheets and large-scale production of fullerene hexagonal nanosheets *J. Am. Chem. Soc.* **131** 9940–4

[33] Shrestha L K, Sathish M, Hill J P, Miyazawa K, Tsuruoka T, Sanchez-Ballester N M, Honma I, Ji Q and Ariga K 2013 Alcohol-induced decomposition of Olmstead's crystalline Ag(I)-fullerene heteronanostructure yields'bucky cubes' *J. Mater. Chem.* C **1** 1174–81

[34] Shrestha L K, Hill J P, Tsuruoka T, Miyazawa K and Ariga K 2013 Surfactant-assisted assembly of fullerene (C_{60}) nanorods and nanotubes formed at a liquid–liquid interface *Langmuir* **29** 7195–202

[35] Shrestha L K, Ji Q, Mori T, Miyazawa K, Yamauchi Y, Hill J P and Ariga K 2013 Fullerene nanoarchitectonics: from zero to higher dimensions *Chem. Asian J.* **8** 1662–79

[36] Shrestha L K, Yamauchi Y, Hill J P, Miyazawa K and Ariga K 2013 Fullerene crystals with bimodal pore architectures consisting of macropores and mesopores *J. Am. Chem. Soc.* **135** 586–9

[37] Shrestha L K, Hill J P, Miyazawa K and Ariga K 2012 Mixing antisolvents induced modulation in the morphology of crystalline C_{60} *J. Nanosci. Nanotechnol.* **12** 6380–4

[38] Sathish M and Miyazawa K 2007 Size-tunable hexagonal fullerene (C_{60}) nanosheets at liquid–liquid interface *J. Am. Chem. Soc.* **129** 13816–7

[39] Miyazawa K and Hotta K 2010 The effect of solvent ratio and water on the growth of C_{60} nanowhiskers *J. Cryst. Growth* **312** 2764–70

[40] Cha S I, Miyazawa K and Kim J-D 2008 Vertically well-aligned C_{60} micro-tube crystal array prepared using solution-based one step process *Chem. Mater.* **20** 1667–9

[41] Miyazawa K, Minato J, Mashino T, Yoshii T, Kizuka T, Kato R, Tachibana M and Suga T 2005 Characterization of the liquid-phase synthesized fullerene nanotubes and nanowhiskers *Proc. of the 2nd JSME/ASME Int. Conf. on Materials and Processing 2005—M&P2005: The 13th JSME Materials and Processing Conf. (Seattle, WA, 19–22 June)* pp (SMS23)-1–4

[42] Miyazawa K, Kuriyama R, Shimomura S, Wakahara T and Tachibana M 2014 Growth and FIB-SEM analyses of C_{60} microtubes vertically synthesized on porous alumina membranes *J. Cryst. Growth* **388** 5–11

[43] Cha S I, Miyazawa K and Kim J 2014 Substrate having fullerene thin wires and method for manufacture thereof *United States Patent* 8685160B2

[44] Amer M S, Todd T K and Busbee J D 2011 Effect of linear alcohol molecular size on the self-assembly of fullerene whiskers *Mater. Chem. Phys.* **130** 90–4

[45] Hotta K and Miyazawa K 2008 Growth rate measurement of C_{60} fullerene nanowhiskers *Nano* **3** 355–9
[46] Asaka K, Kato R, Yoshizaki R, Miyazawa K and Kizuka T 2007 Fracture surface and correlation of buckling force with aspect ratio of C_{60} crystalline whiskers *Diam. Relat. Mater.* **16** 1936–9
[47] Kizuka T, Saito K and Miyazawa K 2008 Young's modulus of crystalline C_{60} nanotubes studied by *in situ* transmission electron microscopy *Diam. Relat. Mater.* **17** 972–4
[48] Saito K, Miyazawa K and Kizuka T 2009 Bending process and Young's modulus of fullerene C_{60} nanowhiskers *Japan. J. Appl. Phys.* **48** 010217
[49] Asaka K, Kato R, Miyazawa K and Kizuka T 2006 Buckling of C_{60} whiskers *Appl. Phys. Lett.* **89** 071912
[50] Kato R and Miyazawa K 2011 Cross-sectional structural analysis of C_{60} nanowhiskers by transmission electron microscopy *Diam. Relat. Mater.* **20** 299–303
[51] Kizuka T, Miyazawa K and Tokumine T 2012 Solvation-assisted Young's modulus control of single-crystal fullerene C_{70} nanowhiskers *J. Nanotechnol.* **2012** 583817
[52] Miyazawa K, Hamamoto K, Nagata S and Suga T 2003 Structural investigation of the C_{60}/C_{70} whiskers fabricated by forming liquid–liquid interfaces of toluene with dissolved C_{60}/C_{70} and isopropyl alcohol *J. Mater. Res.* **18** 1096–103
[53] Minato J, Miyazawa K and Suga T 2005 Morphology of C_{60} nanotubes fabricated by the liquid–liquid interfacial precipitation method *Sci. Technol. Adv. Mater.* **6** 272–7
[54] Ji H-X, Hu J-S, Tang Q-X, Song W-G, Wang C-R, Hu W-P, Wan L-J and Lee S-T 2007 Controllable preparation of submicrometer single-crystal C_{60} rods and tubes through concentration depletion at the surfaces of seeds *J. Phys. Chem.* C **111** 10498–502
[55] Ringor C L and Miyazawa K 2009 Fabrication of solution grown C_{60} fullerene nanotubes with tunable diameter *J. Nanosci. Nanotechnol.* **9** 6560–4
[56] Hotta K and Miyazawa K 2008 Growth rate measurement of C_{60} fullerene nanowhiskers *Nano* **3** 355–9
[57] Tachibana M, Kobayashi K, Uchida T, Kojima K, Tanimura M and Miyazawa K 2003 Photo-assisted growth and polymerization of C_{60} 'nano' whiskers *Chem. Phys. Lett.* **374** 279–85
[58] Kobayashi K, Tachibana M and Kojima K 2005 Photo-assisted growth of C_{60} nanowhiskers from solution *J. Cryst. Growth* **274** 617–21
[59] Miyazawa K and Hotta K 2011 The effect of water on the stability of C_{60} fullerene nanowhiskers *J. Nanopart. Res.* **13** 5739–47
[60] Wei M, Luo H, Li N, Zhang S and Gan L 2002 Study of electrochemical properties of pyrrolidinofullerenes by microelectrode voltammetry *Microchem. J.* **72** 115–112
[61] Wakahara T, Miyazawa K, Nemoto Y and Ito O 2011 Diameter controlled growth of fullerene nanowhiskers and their optical properties *Carbon* **49** 4644–9
[62] Miyazawa K, Hirata C and Wakahara T 2014 Influence of the solution volume on the growth of C_{60} nanowhiskers *J. Cryst. Growth* **405** 68–72
[63] Kawasaki S and Sakai E 1967 Measurement of diffusion of gold in copper by elastic scattering of deuteron *J. Nucl. Sci. Technol.* **4** 273–7
[64] Ogawa K, Kato T, Ikegami A, Tsuji H, Aoki N and Ochiai Y 2006 Electrical properties of field-effect transistors based on C_{60} nanowhiskers *Appl. Phys. Lett.* **88** 112109
[65] Somani P R, Somani S P and Umeno M 2007 Toward organic thick film solar cells: three dimensional bulk heterojunction organic thick film solar cell using fullerene single crystal nanorods *Appl. Phys. Lett.* **91** 173503
[66] Shrestha R G, Shrestha L K, Khan A H, Kumar G S, Acharya S and Ariga K 2014 Demonstration of ultrarapid interfacial formation of 1D fullerene nanorods with photovoltaic properties *Appl. Mater. Interfaces* **6** 15597–603
[67] Cho B H, Lee K B, Miyazawa K and Ko W B 2013 Preparation of fullerene (C_{60}) nanowhisker-ZnO nanocomposites by heat treatment and photocatalytic degradation of methylene blue *Asian J. Chem.* **25** 8027–30
[68] Yang J, Lim H, Choi H C and Shin H S 2010 Wavelength-selective silencing of photocurrent in Au-coated C60 wire hybrid *Chem. Commun.* **46** 2575–7
[69] Li H, Tee B C-K, Cha J J, Cui Y, Chung J W, Lee S Y and Bao Z 2012 High-mobility field-effect transistors from large-area solution-grown aligned C_{60} single crystals *J. Am. Chem. Soc.* **134** 2760–5
[70] Miyazawa K, Kuwasaki Y, Hamamoto K, Nagata S, Obayashi A and Kuwabara M 2003 Structural characterization of the C_{60} nanowhiskers formed by the liquid–liquid interfacial precipitation method *Surf. Interface Anal.* **35** 117–20
[71] Larsson M P, Kjelstrup-Hansen J and Lucyszyn S 2007 Dc characterisation of C_{60} whiskers and nanowhiskers *ECS Trans.* **2** 27–38
[72] Xu M S, Pathak Y, Fujita D, Ringor C and Miyazawa K 2008 Covered conduction of individual C_{60} nanowhiskers *Nanotechnology* **19** 075712
[73] Ji H-X, Hu J-S, Wan L-J, Tang Q-X and Hu W-P 2008 Controllable crystalline structure of fullerene nanorods and transport properties of an individual nanorod *J. Mater. Chem.* **18** 328–32
[74] Hannay N B, Geballe T H, Matthias B T, Andres K, Schmidt P and MacNair D 1965 Superconductivity in graphitic compounds *Phys. Rev. Lett.* **14** 225–6
[75] Koike Y, Suematsu H, Higuchi K and Tanuma S 1980 Superconductivity in graphite–alkali metal intercalation compounds *Physica* B **99** 503–8
[76] Weller T E, Ellerby M, Saxena S S, Smith R P and Skipper N T 2005 Superconductivity in the intercalated graphite compounds C_6Yb and C_6Ca *Nat. Phys.* **1** 39–41
[77] Kato R, Miyazawa K, Nishimura T and Wang Z M 2009 High-resolution transmission electron microscopy of heat-treated C_{60} nanotubes *J. Phys.: Conf. Ser.* **159** 012024
[78] Asaka K, Nakayama T, Miyazawa K and Saito Y 2012 Study on structure of heat-treated fullerene nanowhiskers and their field electron emission characteristics *Surf. Interface Anal.* **44** 780–3
[79] Asaka K, Nakayama T, Miyazawa K and Saito Y 2012 Structures and field emission properties of heat-treated C_{60} fullerene nanowhiskers *Carbon* **50** 1209–15
[80] Ekimov E A, Sidorov V A, Bauer E D, Mel'nik N N, Curro N J, Thompson J D and Stishov S M 2004 Superconductivity in diamond *Nature* **428** 542–5
[81] Takano Y, Nagao M, Sakaguchi I, Tachiki M, Hatano T, Kobayashi K, Umezawa H and Kawarada H 2004 Superconductivity in diamond thin films well above liquid helium temperature *Appl. Phys. Lett.* **85** 2851–3
[82] Hebard A F, Rosseinsky M J, Haddon R C, Murphy D W, Glarum S H, Palstra T T M, Ramirez A P and Kortan A R 1991 Superconductivity at 18 K in potassium-doped C60 *Nature* **350** 600
[83] Tanigaki K, Ebbesen T W, Saito S, Mizuki J, Tsai J S, Kubo Y and Kuroshima S 1991 Superconductivity at 33 K in $Cs_xRb_yC_{60}$ *Nature* **352** 222–3
[84] Haddon R C 1992 Electronic structure, conductivity, and superconductivity of alkali metal doped C_{60} *Acc. Chem. Res.* **25** 127–33
[85] Minato J and Miyazawa K 2005 Solvated structure of C_{60} nanowhiskers *Carbon* **43** 2837–41
[86] Cui W *et al* 2011 Synthesis of alkali-metal-doped C_{60} nanotubes *Diam. Relat. Mater.* **20** 93–6

[87] Takeya H, Miyazawa K, Kato R, Wakahara T, Ozaki T, Okazaki H, Yamaguchi T and Takano Y 2012 Superconducting fullerene nanowhiskers *Molecules* **17** 4851–9
[88] Takeya H, Kato R, Wakahara T, Miyazawa K, Yamaguchi T, Ozaki T, Okazaki H and Takano Y 2013 Preparation and superconductivity of potassium-doped fullerene nanowhiskers *Mater. Res. Bull.* **48** 343–5
[89] Murphy D W, Rosseinsky M J, Haddon R C, Ramirez A P, Hebard A F, Tycko R, Fleming R M and Dabbagh G 1991 Superconductivity in alkali metal fullerides *Physica* C **185–9** 403–7
[90] Takeya H, Miyazawa K and Takano Y 2012 Development of alkali-metal doped superconducting fullerene nanowhiskers *Mater. Integr.* **25** 38–44 (in Japanese)
[91] Butterman W C and Reese R G Jr 2003 *Mineral Commodity Profiles—Rubidium* (*US Geological Survey Open-File Report* 03-045)
[92] Wakahara T, Angelo P D', Miyazawa K, Nemoto Y and Ito O 2012 Fullerene/cobalt porphyrin hybrid nanosheets with ambipolar charge transporting characteristics *J. Am. Chem. Soc.* **134** 7204–6
[93] Barzegar H R, Larsen C, Edman L and Wågberg T 2013 Solution-based phototransformation of C_{60} nanorods: towards improved electronic devices *Part. Part. Syst. Charact.* **30** 715–20
[94] Larsen C, Barzegar H R, Nitze F, Wågberg T and Edman L 2012 On the fabrication of crystalline C_{60} nanorod transistors from solution *Nanotechnology* **23** 344015
[95] Doi T, Koyama K, Chiba Y, Tsuji H, Ueno M, Chen S-R, Aoki N, Bird J P and Ochiai Y 2010 Electron transport properties in photo and supersonic wave irradiated C_{60} fullerene nano-whisker field-effect transistors *Japan. J. Appl. Phys.* **49** 04DN12
[96] Cui H *et al* 2014 High-temperature calcined fullerene nanowhiskers as well as long needle-like multi-wall carbon nanotubes have abilities to induce NLRP3-mediated IL-1β secretion *Biochem. Biophys. Res. Commun.* **452** 593–9

Journal of the Society of Inorganic Materials, Japan 22, 92–98 (2015)

液–液界面析出法(LLIP 法)によるフラーレンのナノウィスカー・ナノチューブ・ナノシートの合成*

宮 澤 薫 一**

1 はじめに

C_{60} が 1985 年に発見されてより[1]，C_{60} のみならず C_{70} や内包フラーレンを用いた様々な形状の分子結晶が合成されている．筆者らは 2001 年にチタン酸ジルコン酸鉛のコロイド溶液中に C_{60} を添加する研究において C_{60} フラーレンナノウィスカーを見出して以来[2]，液–液界面析出法(liquid-liquid interfacial precipitation method, LLIP 法)によって[3]，様々な形状のフラーレン結晶の合成を行っている．本稿では，筆者らが開発した LLIP 法の原理と LLIP 法によるファイバーおよびシート状のフラーレン結晶の合成例について述べる．

2 液–液界面析出法(LLIP 法)

液–液界面析出法とは，フラーレンの良溶媒(A)の飽和溶液①にフラーレンの貧溶媒(B)を重層し，この過飽和となった液–液界面において生じるフラーレン結晶核の析出と，さらなる良溶媒–貧溶媒の相互拡散によるフラーレンの過飽和状態の維持によって，フラーレン結晶核の成長を行わせる方法である[3,4]．良溶媒 A と貧溶媒 B は互いに混和するものを用いるが，図 1 に示す LLIP 法においては，①に B を，B を①に重層しても良い．あるいは，B の内部に①を注入しても，逆に，①の内部に B を注入しても良く，さらにまた，B に①を，①を B に滴下する形で添加しても良い．重要なことは，①と B の 2 液を合わせる過程においては，必ず液–液界面が形成され(図 1(a))，その界面における相互拡散によってフラーレンの過飽和状態が生じ(図 1(b))，フラーレン結晶核が発生する現象を用いることが，LLIP 法の意図するところである．LLIP 法は，実質的には 2 液を混合する方法であるが，図 1(a)のように，液–液界面をひとつだけ形成するときのみならず，図 1(c)のように，注入などの方法によって導入された小さな貧溶媒体積 B の周りに，溶液①と貧溶媒 B の液–液界面が必然的に

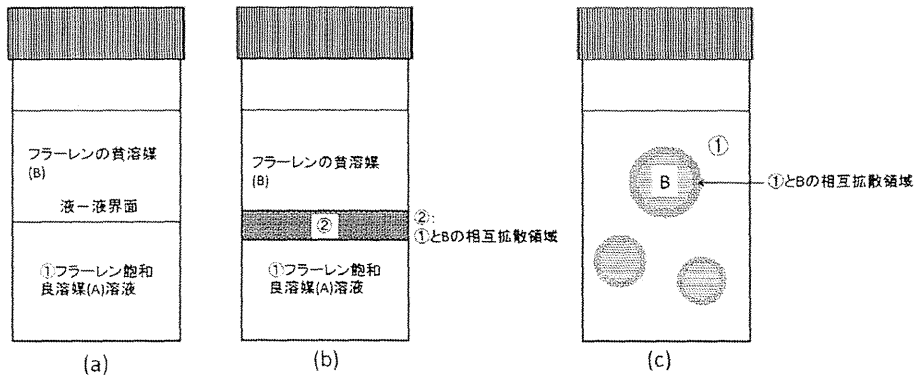

図 1 (a)フラーレンを飽和させた良溶媒(A)溶液①に，フラーレンの貧溶媒(B)を重層した模式図，(b)溶液①と貧溶媒 B との相互拡散領域②，(c)溶液①の中に溶媒 B を注入して生じる球状の領域と溶液①との液–液界面において，過飽和領域が生じることを示す模式図

* Synthesis of Fullerene Nanowhiskers, Fullerene Nanotubes and Fullerene Nanosheets by Liquid-Liquid Interfacial Precipitation (LLIP) Method

** Kun'ichi MIYAZAWA

生じ，引き続き起こる相互拡散によって過飽和領域が形成されるため，このような場合をも含めてLLIP法と呼んでいる．図1のように液-液界面を形成しそのまま拡散と結晶成長を行わせる方法を静置液-液界面析出法(static liquid-liquid interfacial precipitation method，静置LLIP法)とも呼ぶ[4]．

3　フラーレンナノウィスカーの合成

フラーレンナノウィスカー(fullerene nanowhisker，FNW)とは，フラーレン分子から成る細いファイバー状結晶(ウィスカー)であって，直径が1000 nm未満のものである[5]．LLIP法を用いて，C_{60}(フラーレン)ナノウィスカー，C_{70}(フラーレン)ナノウィスカー[2)-6),8)]のようなFNWの他に，C_{60}［$C(COOC_2H_5)_2$］のようなフラーレンの誘導体を用いたFNWの合成も可能である[7),9),10)]．また，LLIP法を用いて，C_{60}母相中にC_{70}を固溶させたFNWや，C_{60}母相中にC_{60}［$C(COOC_2H_5)_2$］や$C_{60}C_3H_7N$を固溶させた複数種類のフラーレン分子から成るFNWを合成することも可能である[9),10)]．

図2にC_{60}母相中にC_{60}［$C(COOC_2H_5)_2$］を固溶させたC_{60}-C_{60}［$C(COOC_2H_5)_2$］2成分ナノウィスカーの透過電子顕微鏡(TEM)像を示す[10)]．

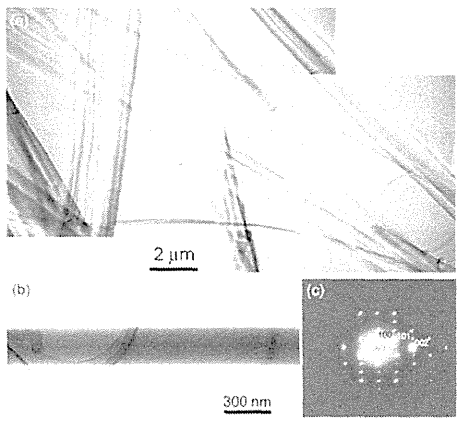

図2　(a)C_{60}-4.1 mol% C_{60}［$C(COOC_2H_5)_2$］粉末を用いて合成された2成分FNWのTEM像，(b)同FNW一部のTEM像とその電子線回折図形(c)[10)]

4　フラーレンナノチューブの合成

フラーレンナノウィスカーは，中空でないフラーレンの細い針状結晶であるのに対して，フラーレンナノチューブ(FNT)とは，フラーレン分子から構成される中空の針状物質である．FNTは，陽極酸化アルミナ膜(AAO膜)の膜孔中にC_{60}のトルエン溶液を侵入させ，それを乾燥，焼成するというプロセスを経て，膜孔の内壁をC_{60}でコーティングし，最後に化学的処理によってアルミナ膜を溶解除去することによって中空の構造をもつ針状物質が合成された[11)]．このようにして合成されるC_{60}ナノチューブ(C_{60}NT)の直径はAAO膜孔の大きさによって規定された揃った直径をもつという利点があるが，多結晶や非晶質構造のものであった．一方，筆者らはC_{70}のピリジン飽和溶液とイソプロピルアルコール(IPA)の静置LLIP法によって，単結晶の壁構造をもつファイバー状のC_{70}ナノチューブ(C_{70}NT)の合成に成功した[12),17)]．同時に，C_{70}を約15 mol%固溶させた単結晶の壁構造をもつC_{60}-C_{70}2成分ナノチューブの合成にも成功した[12)]．C_{60}NTは，C_{60}のピリジン飽和溶液とIPAの静的LLIP法により合成することができるが[13)]，収率を向上させるため，紫外線や青色光で照射したC_{60}飽和ピリジン溶液を用いて，液-液界面を形成後，超音波照射を施すことによってC_{60}NTを合成する方法を開発した[14)]．この方法は，静置LLIP法に超音波による強制混合プロセスを付加した方法であるので，強制混合液-液界面析出法(forced mixing liquid-liquid interfacial precipitation method，強制混合LLIP法)と呼んでいる．

今日まで様々なFNWやFNTがLLIP法によって合成されており，FNWとFNTをひとまとめにしてフラーレンナノファイバーとも呼んでいる[15),16)]．

図3にC_{60}NTの光学顕微鏡像とTEM像[14)]を，図4にC_{70}NTのTEM像を示す[12)]．

5　フラーレンナノシートの合成

Sathishらはフラーレンの良溶媒と貧溶媒の組合せを適当に選択することにより，ファイバー状のみならず薄いシート状の物質を合成した[18)]．これをフラー

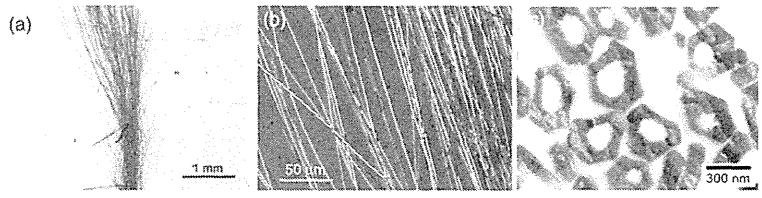

図3　C_{60}NTの光学顕微鏡像(a)，(b)と，C_{60}NTの断面TEM像(c)[14)]

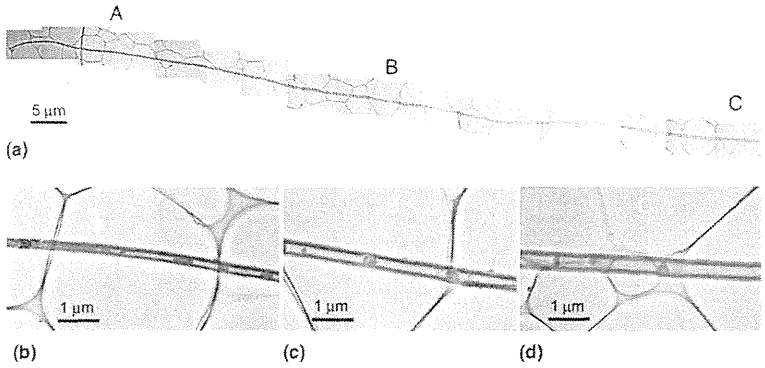

図4　C_{70}NT の TEM 像(a)と，A, B, C 部分の拡大像(b), (c), (d)[12]

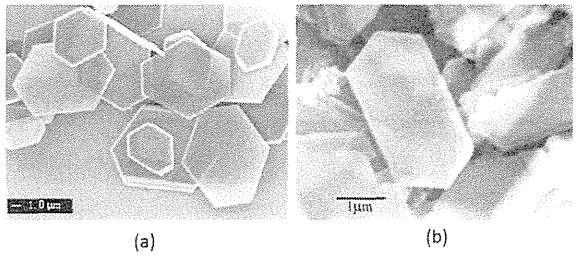

図5　(a)C_{60} ナノシート[19]と(b)C_{70} ナノシート[20]の SEM 像

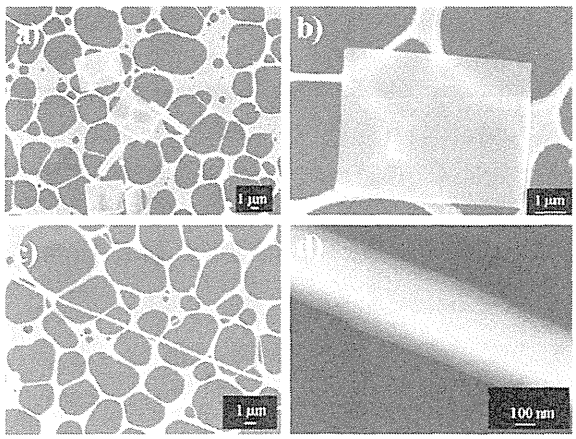

図6　$Sc_3N@C_{80}$ ナノシートの SEM 像 a), b). $Sc_3N@C_{80}$ ナノウィスカーの SEM 像 c)と拡大像 d)[21]

レンナノシートと呼んでいる．次いで若原らによって，LLIP 法においてフェロセンを添加することによりフラーレンナノシートの合成が容易にできることが発見された[19]．図5(a)に C_{60} ナノシートの[19]，図5(b)に C_{70} ナノシート[20]の走査電子顕微鏡(SEM)像を示す．この C_{60} ナノシートは，C_{60} とフェロセンのトルエン溶液と IPA の LLIP 法により合成されたもの[19]，また，C_{70} ナノシートは，C_{70} とフェロセンのトルエン溶液と IPA の LLIP 法によって合成されたものである[20]．

図6に，内包フラーレン $Sc_3N@C_{80}$ と CS_2 および IPA を用いて，LLIP 法により合成された $Sc_3N@C_{80}$ ナノシートと $Sc_3N@C_{80}$ ナノウィスカーの走査電子顕微鏡(SEM)像を示す[21]．

Co ポルフィリン(5,10,15,20-tetrakis(4-methoxyphenyl) porphyrinato cobalt(II)，CoTMPP))を添加した C_{60} ナノシートも合成された[22]．この合成は，C_{60} と CoTMPP のトルエン溶液と IPA の LLIP 法による．CoTMPP 添加 C_{60} ナノシートを用いてアンバイポーラ特性を示す電界効果トランジスター(FET)が作製された．CoTMPP 添加 C_{60} ナノシートの厚さは，原子間力顕微鏡(AFM)の測定により約 50～200 nm であった[22]．

6　垂直配向フラーレンマイクロチューブの合成

陽極酸化アルミナ膜(AAO)の膜孔を通じて，C_{60} 飽和トルエン溶液に IPA をゆっくりと注入することにより，アルミナ膜上に，直径がマイクロメートルサイズの C_{60}(フラーレン)マイクロチューブ(C_{60}MT)を合成することができる[23,24]．図7にその合成方法(diaphragm liquid-liquid interfacial precipitation (DLLIP) method，隔膜液-液界面析出法[24])と C_{60}MT の SEM 像を，図8に集束イオンビーム加工観察装置(FIB-SEM，Hitachi NB5000)による観察例と，図9に C_{60}MT の縦断面 SEM 像を示す．C_{60}MT は AAO 膜上に約 400～500 μm の長さにまで成長している．成長軸方向に沿っての観察像からわかるように(図7(c))，C_{60}MT は六角柱の断面形状をもつ柱状晶である．図9は，C_{60}MT と AAO 膜の接合部近傍では中空でないが，成長するにつれて中空部が形成されることを示している．これは C_{60}MT の外表面の成長速度が大きいために内部への C_{60} の供給が十分でなく中空構造が形成されたと考察することができる．成長に伴って溶液中の C_{60} は消費されて C_{60} 濃度が減少することを考慮すると，C_{60} 濃度の減少によって内部への C_{60} の供給が十分に行われないために中空構造が形成されたと推察している．また，C_{60} の過飽和状態を

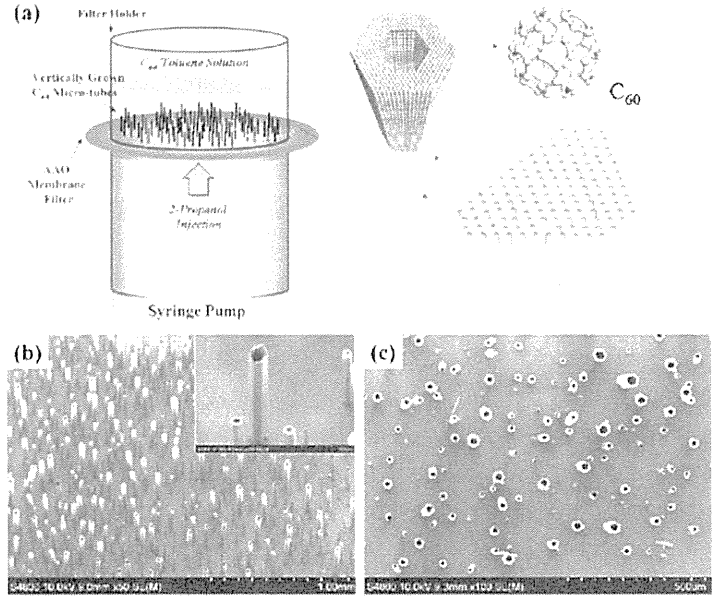

図7 AAO膜の膜孔を通じてC_{60}飽和トルエン溶液中にIPAを注入するDLLIP法によるC_{60}MTの合成方法の模式図(a)と，垂直配向C_{60}MTのSEM像(b)，(c)[23]

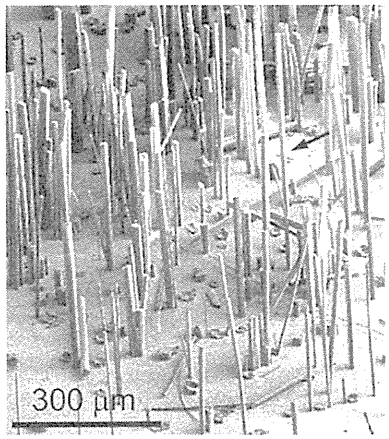

図8 DLLIP法によりAAO膜上に合成された垂直配向C_{60}MTのSEM像[21]

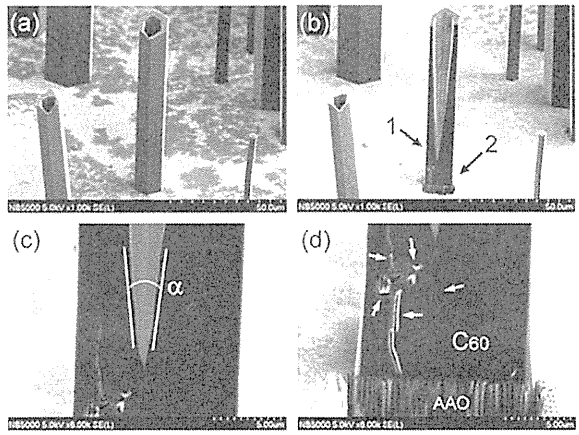

図9 C_{60}MTのSEM像(a)，(a)の中央のC_{60}MTをGaイオンビームで加工して縦断面を形成したC_{60}MTのSEM像(b)，(b)の矢印1で示した近傍の拡大像(c)，AAO膜とC_{60}MT接合界面近傍のSEM像(d)[21]
角度$\alpha=14°$．図(d)の矢印は空隙を示す．

もたらすIPAはC_{60}結晶核の外側から供給されるので，結晶表面に比べて針状結晶内部の成長が遅れることが考えられる．さらに，C_{60}MTの成長に伴って溶液中におけるC_{60}は消費されるため，この結果生じるC_{60}濃度の減少はC_{60}針状結晶コア部分の再溶解を引き起して中空構造を形成することも考えられる[30]．C_{60}MTの成長には，上記のプロセスが複雑に寄与していると考察される．

C_{60}NTやC_{70}NTなどのFNTの形成においても，外表面先端部における成長速度に対して，溶液中におけるフラーレン濃度の減少によって，内部へのフラーレンの供給と結晶化が十分な速さで行われないために中空構造が形成されると考えられる[25]．図4のC_{70}NTのTEM像で示すように[12]，C_{70}NTの端部は閉じた構造をもっており，図4(b)の矢印で示された場所から中空構造が形成されている．これは上記の考察を裏付けている．また，C_{70}NTの内部から溶出したような例も観察されているため[12]，C_{70}NWの中央部分の溶解による中空構造の形成(コア溶解モデル)も考えられる．従って，FNTの形成は，フラーレン分子の結晶表面への供給とその結晶化過程，および，内部コア溶解過程の因子が複雑に関係して生じていると推察される．